Gap junctions deliver malonyl-CoA from soma to germline to support embryogenesis in *Caenorhabditis elegans*

Todd A. Starich[1,2] and David Greenstein[1]

[1]Department of Genetics, Cell Biology and Development, University of Minnesota, Minneapolis, Minnesota 55455 USA

[2]Email: stari001@umn.edu

Abstract

Gap junctions are virtually ubiquitous in metazoans and play critical roles in many important biological processes, including electrical conduction and development. Despite this ubiquity, only a small number of molecules passing through gap junction channels have been definitively linked to specific functions. We isolated gap junction channel mutants that reduce junctional coupling between the soma and germ cells in the *C. elegans* gonad. We use genetic methods to show that malonyl-CoA, the rate-limiting substrate for fatty acid synthesis (FAS), is produced in the soma and delivered through gap junctions to the germline; there it is used by fatty acid synthase to critically support embryonic development. Tissue separation of malonyl-CoA production from its site of utilization facilitates somatic control of germline development and reproduction. Further, our results suggest that this metabolic outsourcing may be a strategy by which the soma communicates nutritional status to the germline.

22 Gap junctions are clusters of intercellular channels allowing direct passage
23 of small molecules between coupled cells. They are widespread in multicellular
24 organisms, though different gene families encode the protein subunits in
25 invertebrates (innexins) and vertebrates (primarily connexins)[1]. While the
26 capability of small molecules to pass through gap junctions can be shown readily
27 in cultured cells, identification of essential molecules that must pass through
28 channels *in vivo* is challenging. Additionally, disruption of gap junction coupling
29 can affect cell adhesion[2], and resultant defects in intercellular communication
30 may not necessarily relate to the passage of molecules through junctional
31 channels.
32 In *C. elegans*, germ cells are coupled throughout their development to the
33 somatic gonad by gap junctions[3]. Germ cells progress in assembly-line fashion
34 through the early stages of meiosis (Fig. 1a). Gonadal gap junctions have been
35 implicated in germ cell proliferation, oocyte growth, regulation of oocyte meiotic
36 maturation, early embryogenesis and sperm guidance[3-7]. Gap junction
37 hemichannels (half-channels) in the somatic gonad are comprised of the recently
38 duplicated innexins INX-8 and INX-9; apposing germ cell hemichannels are
39 heteromeric and consist of INX-14 in conjunction with either INX-21 or INX-22
40 (Supplementary Fig. 1). Germ cells fail to proliferate in *inx-8(0) inx-9(0)* mutants,
41 at a point upstream of, or parallel to, GLP-1/Notch activation of germ cells by
42 Delta class ligands LAG-2 and APX-1. These ligands are produced in the distal
43 tip cell (DTC) that maintains the proliferative stem cell niche[4,8-10].

44 Germ cell proliferation can be rescued in *inx-8(0) inx-9(0)* mutants to half
45 the level of wild type by driving *inx-8* expression in the DTC with the *lag-2*
46 promoter[3]. In these animals, gap junctions between soma and germline are
47 established in the distal gonad arm, but ostensibly not in the proximal arm; many
48 resultant embryos exhibit characteristics of the Pod phenotype (Polarity and
49 Osmotic sensitivity Defect)[11], including eggshell and permeability barrier
50 deficiencies, cytokinesis failures, and polar body extrusion defects. Other genes
51 with mutations producing Pod embryos include those involved in eggshell
52 synthesis, fatty acid synthesis (FAS), the APC/separase pathway, and a coronin-
53 like protein[11-18].
54 Molecules moving through soma-germ cell gap junctions necessary for
55 proliferation and early embryogenesis are unknown. We use genetic methods to
56 show that malonyl-CoA (mal-CoA) is produced by *pod-2* (acetyl-CoA
57 carboxylase, ACC) in the soma. Transfer of mal-CoA to the germline, for use by
58 *fasn-1* (fatty acid synthase, FASN), is impacted by the integrity of INX-8-
59 containing channels under conditions in which gap junction formation appears
60 normal. Rescue of the Pod phenotype in *pod-2* genetic mosaics indicates a
61 somatic sheath focus of action. Our results support the model that mal-CoA
62 transits from soma to germline through gap junction channels.
63
64
65

66 **Results**

67 *Gametogenesis is delayed by the inx-8(tn1513 tn1555) reduction of function (rf)*
68 *mutation*

69 We previously isolated (in an *inx-9* null background) a strong loss-of-
70 function *inx-8* allele *(tn1513)* with sufficient residual function to contribute to
71 channel formation and cell adhesion but not to support germ cell proliferation[3].
72 *tn1513* encodes a T239I change in the second extracellular loop of the innexin
73 monomer, predicted to be involved in docking with octameric hemichannels on
74 apposing cells (Supplementary Fig. 1)[19]. Using this allele in a genetic screen for
75 restoration of germ cell proliferation, six *inx-8* intragenic suppressor mutations
76 were isolated (to be described elsewhere). One of these, *tn1555*, encodes a
77 D24N change in the amino terminus (Supplementary Fig. 1), near a site that may
78 associate with a cytoplasmic dome structure surrounding the hemichannel outer
79 pore[19]. *inx-8(tn1513 tn1555rf)*--for brevity to be referred to as *inx-8(rf)*--partially
80 restored germ cell numbers and fertility to one-third the level of wild type
81 (Supplementary Table 1). *inx-8(rf)* is rescued by an *inx-8(+)* extrachromosomal
82 array, and rescue of *inx-8(0) inx-9(0)* with an *inx-8(rf)::gfp* array mimics the
83 phenotype of the suppressor mutant; therefore observed phenotypes can be
84 attributed to *inx-8(rf)* and not to other possible background mutations.

85 There is an ~18 hr delay to the onset of fertilization in *inx-8(rf)* compared
86 to wild type, as determined by relating the timing of first ovulation to the L4 molt
87 (L4-to-adult transition) (Fig. 1b). This delay correlates with late expression of

88 *gfp::lin41* in relation to L4 sub-stages of vulval development[20]; LIN-41 is the
89 earliest known marker of oogenesis[21]. In wild type at 20°C, *gfp::lin41* appears by
90 sub-stage L4.7 (Fig. 1c); in *inx-8(rf)*, *gfp::lin41* is expressed after completion of
91 vulval morphogenesis but prior to the L4 molt (Fig. 1c; Supplementary Table 2).
92 Spermatogenesis is also delayed—wild-type sperm appear as early as the L4.7
93 stage, but *inx-8(rf)* sperm first appear after completion of vulval morphogenesis
94 (Supplementary Table 2). Once started, egg-laying in *inx-8(rf)* continues apace
95 such that ~99% of progeny are laid within a 96-hour window (3144/3179 larvae;
96 n=25), similar to wild type (5847/5929 larvae; n=21).
97
98 *inx-8(rf) gap junction formation is more severely affected in proximal gonad arms*
99 To examine expression of INX-8(T239I D24N) mutant innexins encoded
100 by *inx-8(rf)*, specific antibodies were used to label somatic (anti-INX-8) or the two
101 classes of germline (anti-INX-21 or anti-INX-22) hemichannels. In wild-type
102 hermaphrodites, clusters of gap junction puncta form between somatic DTC or
103 sheath cells and each underlying germ cell (Fig. 2a). In distal arms of wild type,
104 loosely clustered sheath-germ cell gap junctions form more basally on germ cells;
105 in *inx-8(rf)* distal arms, both INX-21 and INX-22 puncta tend to localize more
106 laterally, where the sheath cells dip down between adjacent germ cells (Fig. 2b).
107 In the loop region (transition from meiotic pachytene to diplotene), large, higher-
108 order clusters of gap junction puncta form in wild-type animals; these are absent
109 in *inx-8(rf)* (Fig. 2c). In wild-type proximal arms (diakinesis), developing oocytes

110 exhibit extensive formation of INX-22 gap junction puncta, while INX-21 puncta
111 become faint; in *inx-8(rf)* proximal arms, INX-22 and INX-8 are strongly but
112 diffusely expressed, with little co-localization evident (Fig. 2d). These results
113 suggest there may be little gap junction coupling in *inx-8(rf)* proximal arms. We
114 showed previously that sheath-oocyte gap junctions are endocytosed by the
115 oocyte during ovulation[3]. Embryos from *inx-8(0) inx-9(0)* rescued with *inx-*
116 *8(rf)::gfp* show internalized GFP puncta, confirming that *inx-8(rf)* establishes at
117 least some sheath-oocyte gap junctions in the proximal arm (Supplementary Fig.
118 2).

119 Reduced proximal arm expression of gap junctions is seen in *inx-8(0) inx-*
120 *9(0); Ex[lag-2p::inx-8::gfp]* animals—simplified to *inx-8/9(0); Ex[inx-8(DTC+, Sh-*
121 *)]*–which are rescued for germ cell proliferation by driving expression of INX-
122 8::GFP in the DTC, but not sheath (Sh), using the *lag-2* promoter[3]. These
123 animals produce primarily dead embryos, many with Pod characteristics (Table
124 1). In contrast to *inx-8(rf)*, these embryos do not show evidence of *inx-8::gfp*
125 endocytosis, consistent with absence of proximal arm sheath-germline gap
126 junction coupling (Supplementary Fig. 2). *inx-8/9(0); Ex[inx-8(DTC+, Sh-)]*
127 animals also show delayed onset of *gfp::lin41* expression, similar to *inx-8(rf)* (Fig.
128 1c, Supplementary Table 2).

129 We conclude that delayed gametogenesis in *inx-8(rf)* mutants arises from
130 compromised soma-germline gap junction communication, due to altered channel
131 properties that influence the formation and localization of gap junctions,

132 especially in the loop and proximal arm. These regions are additionally implicated
133 because DTC expression of wild-type INX-8 fails to rescue *inx-8(rf)* phenotypes
134 (n>20).
135
136 *inx-8(rf) interacts with FAS mutants*
137 Because *inx-8/9(0); Ex[inx-8(DTC+, Sh-)]* produces Pod-like embryos, and
138 *inx-8(rf)* shows reduced proximal arm gap junction coupling similar to *inx-8/9(0);*
139 *Ex[inx-8(DTC+, Sh-)]*, possible genetic interactions between *inx-8(rf)* and other
140 Pod mutants were explored (Supplementary Table 1). Conditional alleles of
141 genes in the FAS pathway (Fig. 3a) were used to construct double mutants with
142 *inx-8(rf)*. Alleles included: *pod-2(ye60)*, a cold-sensitive (*cs*) allele of the *C.*
143 *elegans* acetyl-CoA carboxylase ACC Type 1[16]; a temperature-sensitive (*ts*)
144 allele of fatty acid synthase *fasn-1(g43)*[22]; and *emb-8(hc69)*, a *ts* allele of an
145 NADPH-cytochrome-P450 reductase, likely necessary for reduction of CYP-450
146 enzymes involved in fatty acid modifications[14,16]. Possible interaction between
147 *pod-2(ye60cs)* and *inx-8(rf)* was difficult to assess–*ye60cs* grown at 15°C was
148 quite sensitive to brief handling at room temperature. At a partially restrictive
149 temperature (22°C), *fasn-1(g43ts); inx-8(rf)* and *emb-8(hc69ts); inx-8(rf)* double
150 mutants exhibited markedly reduced brood sizes. Similar reductions in brood size
151 were also apparent in *emb-8(hc69ts); +/inx-8(rf)*, suggesting *emb-8(hc69ts)* might
152 be highly dose-sensitive to *inx-8(+)* levels (Supplementary Table 1).
153

154 *FAS pathway shifts from soma to germline after pod-2*

155 Genetic interactions between *inx-8* and FAS genes could represent activity
156 in the same or parallel pathways. If gap junctions are positioned in the FAS
157 pathway, it might be possible to find a step within the pathway where gene
158 function shifts from a somatic to a germline focus. *C. elegans* is particularly
159 amenable to such an investigation because simple (highly repetitive)
160 extrachromosomal arrays used to rescue gene function tend to express well in
161 the soma, whereas arrays with more sequence complexity are generally required
162 to prevent silencing of multi-copy gene expression in the germline[23].

163 Previous characterization of *pod-2* implied rescue by a simple array[16]; we
164 likewise found that *pod-2(ye60cs)* is rescued by simple extrachromosomal arrays
165 at 15°C (see Methods). In contrast, 2 fosmids encoding *emb-8*, used individually
166 to generate simple arrays, yielded 65 transformed lines, only one of which
167 rescued *emb-8(hc69ts)* at 25°C; the array in this line was eventually silenced. For
168 *fasn-1*, two fosmids used to generate 93 simple array lines and 20 complex array
169 lines failed to rescue *fasn-1(g43ts)*. These results were consistent with a model in
170 which FAS affecting embryonic development requires *pod-2* in the soma, but
171 shifts to a germline requirement for *fasn-1* and *emb-8*.

172 To avoid misrepresentation of rescue results due to the special nature of a
173 conditional allele, null alleles of *pod-2(tn1691)* and *fasn-1(tn1762)*–simplified to
174 *(0)*–were generated using CRISPR-Cas9 methodology (Fig. 3b,c)[24]. *pod-2(0)*
175 embryos from *pod-2(0)/+* parents arrest late in embryogenesis (pretzel stage;

176 Fig. 3d); most *fasn-1(0)* embryos from *fasn-1(0)/+* parents shows signs of
177 differentiation, and many arrest late in embryogenesis; occasional hatchlings
178 emerge with probable hypodermal defects (see below). *pod-2(0)* was rescued by
179 simple extrachromosomal arrays, supporting probable somatic function. Using a
180 PCR-amplified genomic fragment we were able to rescue somatic but not
181 germline function of *fasn-1(0)* with a simple or complex array (see Methods). A
182 genetically-balanced line with a complex array, *hT2/ fasn-1(0)*; *Ex[fasn-1(+); sur-*
183 *5::gfp(+)]*, segregates healthy homozygous *fasn-1(0); Ex[fasn-1(+); sur-5::gfp(+)]*
184 adults that lay almost exclusively Pod embryos (Table 1). (*sur-5::gfp* is a co-
185 injection marker expressed in somatic cell nuclei; corresponding
186 extrachromosomal arrays can be lost mitotically to generate mosaics—see
187 below[25].) Gonad arms appear normal, and animals lay wild-type numbers of
188 defective embryos (Table 1); many of these display polarity defects (4/14
189 symmetric first divisions) and exhibit extra nuclei in early embryos (Fig. 3e-h).
190 Embryos typically arrest prior to morphogenesis. We conclude this *fasn-1(+)* PCR
191 fragment rescues somatic *fasn-1* function and is either silenced in the germline or
192 lacks an element necessary for germline expression; in either case a germline
193 requirement is indicated. In sum, rescue results are consistent with a fertility
194 requirement for *pod-2* in the somatic gonad and *fasn-1* in the germline. This
195 conclusion is supported by genetic mosaic and gene expression data described
196 below. If *inx-8* gap junctions act in this pathway, it would position these junctions

197 between *pod-2* and *fasn-1* as possible mediators of mal-CoA transfer from soma
198 to germline.
199
200 *GFP::POD-2 and GFP::FASN-1 are tissue restricted*
201 Endogenous, homozygous-viable, fertile GFP-labeled alleles of *pod-2* and
202 *fasn-1* were generated to determine if patterns of localization are consistent with
203 predicted foci of action. The GFP moiety in *gfp::pod-2(tn1765)* is expected to
204 label all 3 predicted isoforms (Fig. 3b)[26]. GFP::POD-2 expression is strongest in
205 the intestine, and prominent in the hypodermis, gonadal sheath (especially
206 proximal sheath), CAN neuron, and excretory duct (Supplementary Fig. 3).
207 GFP::POD-2 expression decreases in response to starvation (Supplementary
208 Fig. 3).
209 *gfp::fasn-1(tn1782)* labeled at the amino terminus (Fig. 3c) is expressed
210 in the hypodermis, gonad sheath (esp. proximal) and excretory duct; intestinal
211 and CAN neuron expression are not evident (Supplementary Fig. 4). This
212 expression pattern partially overlaps with that of a *fasn-1* promoter::GFP reporter
213 which was expressed in the intestine[27]. WormBase[26] predicts a single FASN-1
214 isoform, but a second in-frame ATG lies in Exon 2; intestinal FASN-1 could be
215 derived from translational initiation at this site, which would not be revealed in our
216 construct. Attempts to GFP-label FASN-1 downstream of this second ATG, or at
217 the C-terminus, were unsuccessful. Neither *gfp::pod-2* nor *gfp::fasn-1* is
218 expressed in the DTC.

219 Germline expression for either GFP-tagged gene was not detected. Anti-
220 GFP staining of dissected gonads failed to detect germline GFP expression
221 (Supplementary Fig. 3). The earliest detectable GFP::FASN-1 in embryos
222 appears in developing hypodermis; GFP::POD-2 is prominent in developing
223 hypodermis and intestine (Supplementary Fig. 3,4). Expression of both genes is
224 consistent with primarily somatic functions. Germline *fasn-1* activity may derive
225 from low levels of expression, though its presence is confirmed by the late arrest
226 phenotype of *fasn-1(0)* embryos derived from *+/fasn-1(0)* parents
227 (Supplementary Fig. 4, e-h).
228
229 *inx-8 channels influence effects of overexpressed malonyl-CoA on downstream*
230 *FAS mutations*
231 If *inx-8* is required for transit of mal-CoA from soma to germline through
232 gap junctions, the fertility of mutants downstream of *pod-2* in the FAS pathway
233 could be compromised by inclusion of INX-8(T239I D24N) into somatic
234 hemichannels. Expression of an *Ex[pod-2(+); sur-5::gfp]* simple array increases
235 the brood size of *emb-8(hc69ts)* at 22°C. This increase is dependent on INX-8
236 hemichannel integrity—*inx-8(+)* homozygotes facilitate the increase more
237 effectively than *+/inx-8(rf)* heterozygotes (Fig. 4a). Importantly, anti-INX-8 and
238 anti-INX-22 co-localization in *emb-8(hc69ts); +/inx-8(rf)* dissected gonads is
239 indistinguishable from wild type, implying that cell adhesion is not affected (Fig.
240 2e).

241 In contrast to *emb-8(hc69ts)*, expression of *Ex[pod-2(+); sur-5::gfp]* in
242 *fasn-1(g43ts)* significantly reduced brood size ($p<0.01$), and brood size reduction
243 is more severe in homozygous *inx-8(+)* than heterozygous *+/inx-8(rf)*
244 backgrounds ($\rho<0.05$) (Fig. 4b). This result likely relates to the mechanism of
245 FASN production of fatty acids--acetyl-CoA (FA chain initiation) and mal-CoA
246 (chain elongation) load at a common, non-selective acyl-CoA binding site and are
247 regarded as competitive inhibitors[28,29]. Increasing the ratio of mal-CoA to acetyl-
248 CoA may inhibit FASN-1 enzyme by interfering with chain initiation. Both wild-
249 type and enhanced levels of mal-CoA delivered through wild-type INX-8
250 hemichannels appear to inhibit *fasn-1(g43ts)*; this mutant form of FASN may be
251 especially sensitive to inhibition by higher levels of mal-CoA. Importantly,
252 heterozygous *+/inx-8(rf)* channels ameliorate this inhibition, likely by reducing
253 mal-CoA transfer.
254 Enhancement by *inx-8(+)* hemichannels of both a positive *(emb-8)* and a
255 negative *(fasn-1)* effect on FAS mutations downstream of overexpressed *pod-*
256 *2(+)* strongly argues that *inx-8* acts in the same pathway as *pod-2*, and is
257 consistent with gap junctions acting as conveyors of mal-CoA from soma to
258 germline (Fig. 4c).
259
260
261

262 *Genetic mosaic analyses associate pod-2 sheath cell loss with the Pod*
263 *phenotype*

264 To verify a somatic *pod-2* focus of action, genetic mosaic animals derived
265 from *pod-2(0); Ex[pod-2(+); sur-5::gfp]* were sought. 17/833 adult hermaphrodites
266 were identified that produced dead eggs but no viable progeny; these adults were
267 examined for cell lineage loss of *Ex[pod-2(+); sur-5::gfp]*. Animals fell into two
268 classes: 1) eight animals lost *Ex[pod-2(+); sur-5::gfp]* from most or all gonad
269 sheath cells, and 2) nine animals lost *Ex[pod-2(+); sur-5::gfp]* from the intestine
270 (Fig. 5a).

271 Within the first class of mosaics, five animals lost the array in all sheath
272 cells in both gonad arms. Three other animals exhibited a difference in
273 phenotypic severity between gonad arms—embryos derived from one arm
274 developed to later multicellular stages *in utero* (Fig. 5b-d). Differences were
275 coincident with loss of the array from all sheath cells in the more severely
276 affected arm, versus retention of the array in a single sheath cell of the better
277 arm. In subsequent screening, five more mosaics were identified that displayed
278 phenotypic disparity between the two gonad arms; in one example, one arm
279 produced defective embryos while the better arm gave rise to wild-type embryos
280 (producing ≥40 viable progeny). These results indicate that the focus of *pod-2(0)*
281 rescue is autonomous to each gonad arm, consistent with the interpretation that
282 *pod-2* expression in the somatic sheath is essential to embryonic viability.

283 In subsequent screening for germline (P_4 –) mosaics, four animals were
284 identified that maintained the array in the soma but lost the array in all embryos
285 (Fig. 5a). The terminal stages of embryonic development resembled those of
286 *pod-2(0)* embryos derived from *+/pod-2(0)* parents, i.e. embryos developed to 3-
287 fold or pretzel stages but failed to hatch (Fig. 5e-g). These stages are more
288 advanced than terminal stages of many dead embryos derived from parents with
289 somatic (but not germline) loss of the rescuing array; such embryos fail to
290 differentiate (Fig. 5h). This early developmental arrest resembles terminal-stage
291 Pod embryos from *fasn-1(0); Ex[fasn-1(+))*] (compare panels h and i in Fig. 5).
292 We conclude that somatic *pod-2(+)* supplies sufficient levels of mal-CoA to the
293 germline not only to establish a wild-type 1-cell embryo, but also to support
294 continued development, presumably until zygotic *pod-2* expression becomes
295 adequate for completion of embryogenesis. These studies establish that
296 metabolites essential for embryonic development can be produced in the somatic
297 gonad and provided to the oocyte through gap junctions.
298
299 *Intestinal loss of pod-2, but not fasn-1, results in a germline starvation response*
300 The other class of *pod-2(0)* genetic mosaics producing dead eggs in our
301 original screen lost *Ex[pod-2(+); sur-5::gfp]* from the intestine (E–) (Fig. 5a). E(–)
302 mosaic animals were smaller than wild type, and gonad arms were severely
303 reduced in size (Fig. 6a). Only the most proximal oocytes showed appreciable
304 growth. E(–) mosaic gonad arms resemble those seen in gonads undergoing the

305 oocyte starvation response, or adult reproductive diapause (ARD), a process
306 induced by starvation during the L4 larval stage proposed to maintain germline
307 stem cells for repopulation of the gonad upon the resumption of feeding[30,31].
308 During ARD, germline stem cells cease dividing, the gonad shrinks due to
309 extensive apoptosis of differentiated germ cells, and growth is largely restricted to
310 the most proximal oocyte.

311 The *C. elegans* intestine is rich with lipid droplets and the source of yolk,
312 and regarded as a major site of FAS[32]. A genetic pathway in *C. elegans* required
313 for intestinal apical polarity establishment leading to proper lumen formation has
314 been described; genes in this pathway, including *pod-2*, encode enzymes
315 required for glycosphingolipid synthesis[33]. Lipid biosynthesis is required
316 throughout larval growth, coincident with membrane expansion. The identification
317 of adult mosaics lacking *pod-2(+)* in the intestine was therefore surprising. We
318 subsequently identified two presumptive P_1(–) *pod-2* mosaics, predicted to have
319 lost *pod-2(+)* function in the intestine, somatic gonad, germline, many muscle and
320 hypodermal cells, among others (Fig. 5a). The most striking phenotype
321 distinguishing these animals from E(–) mosaics was an extremely constipated
322 intestine (Fig. 6b). The absence of this constipation in E(–) mosaic animals
323 implies that loss of *pod-2(+)* from the intestine does not prevent the processing of
324 bacteria through the intestinal lumen. (Both P_1 mosaics showed tissue extruded
325 from the rectum, which may be the cause of constipation.)

326 Although *gfp::fasn-1(tn1782)* is not detected in the intestine, we asked if
327 there is a functional role for *fasn-1* similar to *pod-2*. As described above,
328 homozygous *fasn-1(0); Ex[fasn-1(+); sur-5::gfp]* progeny from heterozygous
329 parents produce Pod embryos but exhibit no other phenotype; within this class of
330 progeny we screened for E(–) mosaics. Ten (of 800) such animals were identified
331 (Fig. 5a); in stark contrast to *pod-2*, their gonad arms appeared normal. These
332 animals displayed no overt defects outside of Pod embryo production (Fig. 6c).
333 Because maternal FASN-1 rescues *fasn-1(0)* homozygotes to later embryonic
334 stages, an early intestinal function for *fasn-1* equivalent to *pod-2* could be
335 rescued maternally. However, the surprising conclusion from this mosaic analysis
336 is that there is no significant intestinal requirement for zygotic *fasn-1* in larval and
337 adult stages. The implication is that the primary function of mal-CoA produced in
338 the intestine may not be as substrate for intestinal FASN-1.
339
340 *Is malonyl-CoA required in other germline processes?*
341 *inx-8(rf)* and *inx-8/9(0); Ex[inx-8(DTC+, Sh-)]* share delayed oogenesis
342 and a reduction in gap junction coupling, germ cell proliferation, and brood size.
343 *inx-21(0)* mutants are sterile, and *inx-22(0)* mutants are fertile[3]; therefore mal-
344 CoA required for embryos must transit through gap junction channels comprised
345 of INX-14/INX-21 hemichannels, which are expressed throughout the distal arm
346 (Fig. 2b). We asked if mal-CoA levels might influence phenotypes preceding
347 embryogenesis, such as oocyte production.

348 Microinjection of mal-CoA (0.5-10 mM) into *inx-8/9(0); Ex[inx-8(DTC+,*
349 *Sh-)]* L4 gonad arms failed to ameliorate phenotypes such as Pod-embryo
350 production or low brood size. Ectopic expression of GFP::POD-2 in the germline
351 in *inx-8/9(0); Ex[inx-8(DTC+, Sh-)]* or *inx-8(rf)* genetic backgrounds also failed to
352 improve phenotypes, including delayed gametogenesis (Supplementary Fig. 5).
353 However, whether endogenous mal-CoA levels are altered under these
354 conditions is uncertain.
355 Effects of global mal-CoA levels were indirectly examined by comparing
356 higher or lower *pod-2(+)* copy number rescue of *pod-2(0)*; numbers of dead eggs
357 and larvae were summed to reflect total embryo output (Table 1). Lower copy
358 number rescue coincided with reduced embryo output (84% of wild-type) and
359 lower proportion of viable larvae within a brood (~37% of total embryos) (Table
360 1). Embryo output may therefore by impacted by *pod-2* expression; however,
361 somatic cells outside the gonad could be responsible. We therefore asked
362 specifically if FA synthesis is required within the germline. Somatically-rescued
363 *fasn-1(0); Ex[fasn-1(+); sur-5::gfp]* embryo output is comparable to wild-type
364 (94%); however, embryo output in the double mutant *fasn-1(0); inx-8(rf); Ex[fasn-*
365 *1(+); sur-5::gfp]* is only ~50% of *inx-8(rf)* alone (Table 1). The FAS pathway may
366 therefore play a germline role affecting embryo output. Surprisingly, *inx-8(rf)*
367 partially suppresses the embryonic lethality of *fasn-1(0); Ex[fasn-1(+); sur-5::gfp]*
368 (Table 1). Possibly the smaller gonad arms of *inx-8(rf)* may concentrate levels of
369 FASN-1 or mal-CoA. Alternatively, *fasn-1* array germline expression may be de-

370 silenced in this genetic background. Further study is needed to address the

371 nature of this suppression.

372 **Discussion**

373 The genetic analysis of mutant *inx-8* soma-germline gap junction channels
374 has led us to three conclusions that have significance beyond the *C. elegans*
375 model system: 1) Mal-CoA produced in the somatic sheath is delivered through
376 gap junctions to the germline; this mal-CoA is necessary to establish a proper
377 one-cell embryo and to support continued embryogenesis. To our knowledge,
378 this segregation of the cellular source of mal-CoA from the eventual cell type in
379 which it is used as substrate is novel. As the rate-limiting step in FAS, mal-CoA
380 production is an attractive control point to tie aspects of germ cell developmental
381 progression to somatic control. 2) *pod-2* expression (and presumably mal-CoA
382 production) is exceptionally robust in the intestine and essential for normal
383 germline development. In the absence of intestinal POD-2, the germline exhibits
384 phenotypic hallmarks of germline ARD despite the presence of a replete food
385 source. By contrast, intestinal *fasn-1* expression is not similarly required. (A
386 possible caveat is that maternal *fasn-1* in the intestine may be sufficient to reach
387 adulthood, which would be surprising.) In light of the abundant expression level of
388 *gfp::pod-2* in the intestine, and our finding that mal-CoA can be directionally
389 transferred intercellularly, the question arises as to whether the intestine provides
390 mal-CoA to other cells. Alternatively, a deficit of mal-CoA production in the
391 intestine might initiate a systemic starvation response. Recently, Gerisch *et al.*
392 (2020)[34] have shown that the HLH-30/TEFB transcription factor functions as a
393 master regulator of the ARD state. *hlh-30* mutants fail to effect the system-wide

394 changes promoting long-term survival and recovery associated with ARD. ARD
395 longevity does not appear to rely on fatty acid metabolism. However, entry of *hlh-*
396 *30* mutants into the ARD state appears normal; therefore effects of decreased
397 mal-CoA expression in the intestine may lie upstream of *hlh-30* activity. 3) A
398 pronounced delay in gametogenesis along with reduction in brood size results
399 from reduced soma-germline gap junction communication; it is unknown if this
400 delay derives from generally slower mitotic or meiotic progression, or from a
401 developmental block at a particular meiotic stage. The nature of potential
402 molecules passing through gap junctions that are responsible for timely meiotic
403 progression is unknown, but mal-CoA has thus far not been implicated.
404 Our results are consistent with other findings in *C. elegans* related to fatty
405 acid metabolism in oocytes. *pod-2*/ACC requires post-translational covalent
406 attachment of biotin for enzymatic activity, and *bpl-1* (*b*iotin *p*rotein *l*igase-1) is
407 the *C. elegans* ortholog of the necessary holocarboxylase synthetase[35]. Mal-CoA
408 provided in the bacterial diet enables *bpl-1* mutants to develop to adulthood, but
409 *de novo* synthesis of polyunsaturated fatty acids (PUFAs) is required for
410 embryonic viability[35]. Our results indicate that mal-CoA supplied for PUFA
411 synthesis (and other FAS) in the early embryo is derived from the somatic sheath
412 via gap junctions. PUFA-dependent prostaglandin signaling from oocytes
413 influences sperm guidance, and reduction of *inx-14* function disrupts this
414 signaling[7,36]. We suggest that reduced levels of mal-CoA delivered to the oocyte

415 through mutant *inx-14*-containing gap junctions may reduce prostaglandin
416 synthesis and its signaling function for sperm migration.
417 At least one route outside of gap junctions may deliver mal-CoA to the
418 germline early in its development. The primordial germ cells Z2 and Z3 associate
419 with a pair of intestinal cells during embryogenesis; contacts are lost before
420 hatching[37,38]. Therefore an early germline requirement for mal-CoA could be
421 fulfilled directly from the intestine. Loss of such a function would be
422 encompassed within the ARD-like phenotype seen in *pod-2* E(–) mosaics.
423 In addition to its metabolic function in FAS, mal-CoA has established roles
424 as a regulatory molecule. It inhibits beta-oxidation of fatty acids by mitochondria.
425 Inhibitory mal-CoA derives from a second acetyl-CoA carboxylase (ACC2),
426 associated with the mitochondrial membrane. Manipulation of mal-CoA levels in
427 the mouse hypothalamus regulates food intake[39]. Regulation is effected through
428 the brain-specific CPT1-c, via a mechanism distinct from the enzymatic activity of
429 other CPT1 enzymes[40,41]. Little information regarding the *C. elegans* ACC2 is
430 known; somatically-delivered mal-CoA could potentially influence germline
431 mitochondrial function.
432 Malonylation as a post-translational lysine modification has recently been
433 described [42]. Malonylation may inhibit target proteins, such as the glyocolytic
434 enzymes glyceraldehyde 3-phosphate dehydrogenase and pyruvate kinase[43].
435 Malonylation of mTOR reduces mTORC1 complex activity, decreasing
436 endothelial cell proliferation and reducing angiogenesis in a human umbilical

437 model[44]. Together these studies and others suggest a potentially pervasive role
438 for mal-CoA in sensing and responding to nutritional status. One trait associated
439 with rapid tumor growth is an increase in FAS, and FASN has been explored as a
440 cancer therapy target[45]. Possibly the ability of mal-CoA to transit through gap
441 junctions might sustain FAS during tumor progression. The discovery that mal-
442 CoA transits through gap junctions from soma to germline may be indicative of
443 other unappreciated intercellular roles for this important molecule.

References

1. Skerrett, I. M., and Williams, J. B. A structural and functional comparison of gap junction channels composed of connexins and innexins. *Develop. Neurobiol.* **77,** 522-547 (2017)
2. Meyer, R. A., Laird, D. W., Revel, J.-P., and Johnson, R. G. Inhibition of gap junctions and adherens junction assembly by connexin and A-CAM antibodies. *J. Cell Biol.* **119,** 179-189.
3. Starich, T. A., Hall, D. H., and Greenstein, D. Two classes of gap junction channels mediate soma-germline interactions essential for germline proliferation and gametogenesis in *C. elegans. Genetics* **198,** 1127–1153 (2014).
4. Nadarajan, S., Govindan, J. A., McGovern, M., Hubbard, E. J., and Greenstein, D. MSP and GLP-1/Notch signaling coordinately regulate actomyosin-dependent cytoplasmic streaming and oocyte growth in *C. elegans*. *Development* **136,** 2223–2234 (2009).
5. Govindan, J. A., Cheng, H., Harris, J. E., and Greenstein, D. $G\alpha_{o/i}$ and $G\alpha_s$ signaling function in parallel with the MSP/Eph receptor to control meiotic diapause in *C. elegans*. *Curr. Biol.* **16,** 257–1268 (2006).
6. Whitten, S. J., and Miller, M. A. The role of gap junctions in *Caenorhabditis elegans* oocyte maturation and fertilization. *Dev. Biol*. **301,** 432–446 (2007).
7. Edmonds, J. W., McKinney, S. L., Prasain, J. K., and Miller, M. A. The gap junctional protein INX-14 functions in oocyte precursors to promote *C. elegans* sperm guidance. *Dev. Biol.* **359,** 47–58 (2011).

8. Austin, J., and Kimble, J. *glp-1* is required in the germ line for regulation of the decision between mitosis and meiosis in *C. elegans*. *Cell* **51**, 589-599 (1987).
9. Austin, J., Kimble, J. Transcript analysis of *glp-1* and *lin-12*, homologous genes required for cell interactions during development of C. elegans. *Cell* **58,** 565-571 (1989).
10. Henderson, S. T., Gao, D., Lambie, E. J., and Kimble, J. *lag-2* may encode a signaling ligand for the GLP-1 and LIN-12 receptors of *C. elegans***.** *Development* **120,** 2913-2924 (1994).
11. Tagawa, A., Rappleye, C. A., and Aroian, R. V. *pod-2*, along with *pod-1*, defines a new class of genes required for polarity in the early *Caenorhabditis elegans* embryo. *Dev. Biol.* **233,** 412–424 (2001).
12. Johnston, W. L., Krizus, A., and Dennis, J. W. The eggshell is required for meiotic fidelity, polar-body extrusion and polarization of the *C. elegans* embryo. *BMC Biol.* **4,** 35 (2006).
13. Olson, S. K., Bishop, J. R., Yates, J. R., Oegema, K., and Esko, J. D. Identification of novel chondroitin proteoglycans in *Caenorhabditis elegans*: embryonic cell division depends on CPG-1 and CPG-2. *J. Cell Biol.* **173,** 985–994 (2006).
14. Benenati G., Penkov, S., Müller-Reichert, T., Entchev, E. V., and Kurzchalia, T. V. Two cytochrome P450s in *Caenorhabditis elegans* are essential for the organization of eggshell, correct execution of meiosis and polarization of the embryo. *Mech. Dev.* **126,** 382–393 (2009).
15. Zhang, Y., Foster, J. M., Nelson, L. S., Ma, D., Carlow, C. K. S. The chitin synthase

genes *chs-1* and *chs-2* are essential for *C. elegans* development and responsible for chitin deposition in the eggshell and pharynx, respectively. *Dev. Biol*. **285,** 330–339 (2005).

16. Rappleye, C. A., Tagawa, A., Le Bot, N., Ahringer, J., and Aroian, R. V. Involvement of fatty acid pathways and cortical interaction of the pronuclear complex in *Caenorhabditis elegans* polarity. *BMC Dev. Biol.* **3,** 8 (2003).
17. Rappleye, C. A., Tagawa, A., Lyczak, R., Bowerman, B., and Aroian, R. V. The anaphase-promoting complex and separin are required for embryonic anterior-posterior axis formation. *Dev. Cell* **2,** 195–206 (2002).
18. Rappleye, C. A., Paredez, A. R., Smith, C. W., McDonald, K. L., and Aroian, R. V. The coronin-like protein POD-1 is required for anterior-posterior axis formation and cellular architecture in the nematode *Caenorhabditis elegans*. *Genes Dev.* **13,** 2838–2851 (1999).
19. Oshima, A., Tani, K., and Fujiyoshi, Y. Atomic structure of the innexin-6 gap junction channel determined by cryo-EM. *Nat. Commun* **7,** 13681 (2016). https://doi.org/10.1038/ncomms13681
20. Mok, D. Z. L., Sternberg, P. W., and Inoue, T. Morphologically defined sub-stages of *C. elegans* vulval development in the fourth larval stage. *BMC Dev. Biol.* **15,** 26 (2015).
21. Spike, C. A., Coetzee, D., Eichten, C., Wang, X., Hansen, D., and Greenstein, D. The NHL-TRIM protein LIN-41 and the OMA RNA-binding proteins antagonistically control the prophase-to-metaphase transition and growth of *C. elegans* oocytes.

Genetics **198,** 1535–1558 (2014).

22. Jaramillo-Lambert, A., Fuchsman, A. S., Fabritius, A. S., Smith, H. E., and Golden, A. Rapid and efficient identification of *Caenorhabditis elegans* legacy mutations using Hawaiian SNP-based mapping and whole-genome sequencing. *G3* **5,** 1007-1019 (2015).
23. Kelly, W. G., Montgomery, M. K., and Fire, A. Distinct requirements for somatic and germline expression of a generally expressed *Caenorhabditis elegans* gene. *Genetics* **146,** 227-238 (1997).
24. Arribere, J. A., *et al*. Efficient marker-free recovery of custom genetic modifications with CRISPR/Cas9 in *Caenorhabditis elegans*. *Genetics* **198,** 837-846 (2014)
25. Yochem, J., Gu. T., and Han, M. A new marker for mosaic analysis in *Caenorhabditis elegans* indicates a fusion between hyp6 and hyp7, two major components of the hypodermis. *Genetics* **149,** 1323-1334 (1998)
26. WormBase (www.wormbase.org)
27. Lee, K.-Z., Kniazeva, M., Han, M., Pujol, N., and Ewbank, J. The fatty-acid synthase *fasn-1* acts upstream of WNK and Ste20/GCK-VI kinases to modulate antimicrobial peptide expression in *C. elegans* epidermis. *Virulence* **1,** 113-122 (2010)
28. Cox, B. G., and Hammes, G. G. Steady-state kinetic study of fatty acid synthase from chicken liver. *Proc. Natl. Acad. Sci.* **80,** 4233-4237 (1983)
29. Chang, S.-I., and Hammes, G. G. Structure and mechanism of action of a multifunctional enzyme: fatty acid synthase. *Acc. Chem. Res.* **23,** 363-369 (1990)
30. Angelo, G., and Van Gilst, M. R. Starvation protects germline stem cells and extends

reproductive longevity in *C. elegans*. *Science* **326,** 954-958 (2009)

31. Seidel, H. S., and Kimble, J. The oogenic germline starvation response in *C. elegans*. *PloS ONE* **6**(12)**,** e28074. (2011)
32. Watts, J. L., and Ristow, M. Lipid and carbohydrate metabolism in *Caenorhabditis elegans*. *Genetics* **207,** 413-446 (2017)
33. Zhang, H., *et al*. Apicobasal domain identities of expanding tubular membranes depend on glycosphingolipid biosynthesis. *Nat. Cell Biol.* **13,** 1189-1201 (2012)
34. Gerisch, B., *et al*. HLH-30/TFEB is a master regulator of reproductive quiescence. *Develop. Cell* **53,** 1-14 (2020)
35. Watts, J. S., Morton, D. G., Kemphues, K. J., and Watts, J. L. The biotin-ligating protein BPL-1 is critical for lipid biosynthesis and polarization of the *Caenorhabditis elegans* embryo. *J. Biol. Chem.* **293,** 610-622 (2018)
36. Kubagawa, H. M., *et al*. Oocyte signals derived from polyunsaturated fatty acids control sperm recruitment *in vivo*. *Nat. Cell Biol*. **8**, 1143-1148 (2006)
37. Sulston, J. E., Schierenberg, E., White, J. G. & Thomson, J. N. The embryonic cell lineage of the nematode *Caenorhabditis elegans*. *Dev. Biol.* **100,** 64–119 (1983).
38. Abdu, Y., Maniscalco, C., Heddleston, J. M., Chew, T.-L., and Nance, J. Developmentally programmed germ cell remodelling by endodermal cell cannibalism. *Nat. Cell Biol.* **18,** 1302-1310 (2016)
39. Wolfgang, M. J., and Lane, M. D. The role of hypothalamic malonyl-CoA in energy homeostasis. *J. Biol. Chem.* **281,** 37265-37269 (2006)
40. Sierra, A. Y., et al. CPT1c is localized in endoplasmic reticulum of neurons and has

carnitine palmitoyltransferase activity. *J. Biol. Chem.* **283,** 6878-6885 (2008)

41. Reilly, P. T., and Mak, T. W. Molecular pathways: tumor cells co-opt the brain-specific metabolism gene *CPT1C* to promote survival. *Clin. Cancer Res.* **18(21)** **(**2012) doi: 10.1158/1078-0432.CCR-11-3281
42. Peng, C., *et al.* The first identification of lysine malonylation substrates and its regulatory enzyme. *Mol. Cell. Proteomics* **10(12)** doi:10.1074/mcp.M111.012658
43. Kulkami, R. A., *et al.* Discovering targets of non-enzymatic acylation by thioester reactivity profiling. *Cell Chem. Biol.* **24,** 231-242 (2017)
44. Bruning, U., *et al*. Impairment of angiogenesis by fatty acid synthase inhibition involves mTOR malonylation. *Cell Metabolism* **28,** 866-880 (2018)
45. Menendez, J. A., and Lupu, R. Fatty acid synthase and the lipogenic phenotype in cancer pathogenesis. *Nature Rev.* **7,** 763-777 (2007)
46. McCarter, J., Bartlett, B., Dang, T., and Schedl, T. Soma-germ cell interactions in *Caenorhabditis elegans*: multiple events of hermaphrodite germline development require the somatic sheath and spermathecal lineages. *Dev. Biol.* **181,** 121-143 (1997).
47. Berman,H. M., *et al*. The protein data bank. *Nuc. Acids Res.* **28,** 235-242 (2000)
48. NGL viewer: web-based molecular graphics for large complexes. Bioinformatics doi:10.1093/bioinformatics/bty419 (2018)
49. Dickinson, D. J., Pani, A. M., Heppert, J. K., Higgins, C. D., and Goldstein, B. Streamlined genome engineering with a self-excising drug selection cassette. *Genetics* **200,** 1035-1049 (2015)

444 **Methods**

445 *Strains*

446 *C. elegans* strains were grown on standard NGM media (plus Nystatin, 6.25 mg/l)
447 with *E. coli* strain OP50 as food source. Temperatures used for conditional
448 mutants are indicated in main text. In addition to the wild-type strain N2, the
449 following alleles were used: Chr. *I*: *fasn-1(g43ts); fasn-1(tn1762null); fasn-*
450 *1(tn1782[gfp::fasn-1]); lin-41(tn1541[gfp::tev::s-tag::lin-41]);* Chr. *II*: *pod-*
451 *2(ye60cs); pod-2(tn1691null); pod-2(tn1765[gfp::tev::3xFLAG::pod-2]);* Chr. *III*:
452 *emb-8(hc69ts); dpy-17(e1295);* Chr. *IV*: *inx-8(tn1474null) inx-9(ok1502null); inx-*
453 *8(tn1513) inx-9(ok1502); inx-8(tn1513 tn1555) inx-9(ok1502)*—a.k.a. *inx-8(rf)* in
454 main text. Balancers used included: *tmC18 [dpy-5(tmIs1236)] I; hT2[bli-4(e937)*
455 *let-?(q782) qIs48] (I:III); mIs11 IV.* Extrachromosomal arrays used included:
456 *tnEx195[inx-8(+) inx-9(+); sur-5::gfp]; tnEx205[lag-2p::inx-8::gfp; str-1::gfp];*
457 *tnEx212[W09B6-pod-2(+)--20 ng/µl—hi copy; sur-5::gfp]; tnEx218[fasn-1(+); sur-*
458 *5::gfp]; tnEx219[W09B6-pod-2(+)--4 ng/µl—lo copy; sur-5::gfp];* and *tnEx221[inx-*
459 *8(tn1513 tn1555); str-1::gfp].*

460

461 *Microinjection rescue of FAS mutants with extrachromosomal arrays*

462 The cosmid W09B6 was used at 50 ng/µl (2 lines) or 20 ng/µl (1 line) with *sur-*
463 *5::gfp* (75 ng/µl) to rescue *pod-2(ye60cs). sur-5::gfp* expression was faint for both
464 lines obtained with 50 ng/µl and these were not further characterized. *pod-*
465 *2(tn1691null)* was rescued by microinjection using W09B6 at 4 ng/µl (5 lines) or

466 by crossing in *tnEx212*. Fosmids WRM0613bD07(10 ng/µl, or 50 ng/µl—1 line
467 that silenced) and WRM067cB03 (25 ng/ul) were used to attempt rescue of *emb-*
468 *8(hc69ts)*. Numerous conditions using fosmids WRM0612bD08 and
469 WRM0614aH05 in simple or complex arrays were used to try to rescue *fasn-*
470 *1(g43ts)* without success. However, FASN enzyme functions as a dimer;
471 formation of dimers between mutant (*g43*) and wild-type monomers might inhibit
472 phenotypic rescue. After *fasn-1(tn1762null)* was generated, somatic but not
473 germline rescue was obtained using a *fasn-1* genomic PCR product forming
474 simple arrays (1 ng/µl + *sur-5::gfp-75* ng/µl, at least 2/6 lines segregated *fasn-*
475 *1(0); Ex[fasn-1(+); sur-5::gfp(+)]* animals that laid only Pod embryos), or a
476 complex array (1 ng/µl + 20 ng/µl *sur-5::gfp* + 100 ng/µl salmon sperm,1 line
477 from 30 injected animals) as described in the main text.
478
479 *Recombinant DNA constructs for isolation of new pod-2 and fasn-1 alleles*
480 Standard CRISPR/Cas-9 methods were used to generate deletions and GFP
481 insertions in *pod-2* and *fasn-1.* For deletions, 100-nt repair templates were
482 synthesized (Ultramers; IDT) and used in a *dpy-10(cn64)* co-conversion strategy
483 previously described[24]. Injection mixes included: pDD162 (Cas9), 50 ng/µl; 25 ng/µl
484 (*pod-2*) or 10 ng/µl (*fasn-1*) each single guide; Ultramer repair template, 500 nM; *dpy-*
485 *10* single guide (pJA58), 25 ng/µl; *dpy-10(cn64)* Ultramer A2-2F-827, 500nM. Single
486 guides were made by annealing oligo pairs and cloning into pRB1017[24]: Deletions
487 were verified by PCR. The PCR fragment used to rescue *fasn-1(tn1762null)* was

488 amplified from genomic DNA using primers 5'-tacgtcaaacatccgtttgtcaacgtcac-3' and
489 5'-ttcttctcctcgtcctttgatacgaagatc-3'.
490 Generation of GFP insertions into *pod-2* using pDD282 followed established
491 protocols[49]. Injection mix included the single guide (10 ng/µl), repair template (10
492 ng/µl), pDD162 (50 ng/µl), and *sur-5::gfp* (80 ng/µl). The insertion was verified by
493 sequencing PCR products generated with primers positioned outside the homology
494 arms.
495 For *gfp::fasn-1*, we were unable to isolate 3' insertions using the Dickinson
496 method[49]. This method relies on isolation of candidates based on the Roller
497 phenotype, and because *fasn-1* has been implicated in molting, we turned to a co-
498 conversion approach[24]. A repair template was generated that included the GFP
499 sequence from pDD282, and *fasn-1* homology arms on either side. The injection mix
500 contained pDD162, 50 ng/µl; *fasn-1* single guide 10 ng/µl; *gfp::fasn-1* repair template,
501 20 ng/µl; *dpy-10* single guide (pJA58), 25 ng/µl; *dpy-10(cn64)* ultramer A2-2F-827,
502 500nM; and pCFJ190, 2.5 ng/µl. Rol candidates were screened directly for GFP
503 expression. The insertion was verified by sequencing PCR fragments generated
504 using primers placed outside of the repair template sequence (5'-
505 ggaacacaaacattccacatcgccg-3' and 5'-gtgattcatctgaattcgctcactcc-3').
506 *mex-5p::gfp::pod-2::tbb-2-3'UTR* was constructed by Gibson assembly of
507 component PCR products representing the *mex-5* promoter, the "a" isoform of
508 *gfp::pod-2*, and the tbb-2-3'UTR to prevent germline RNA degradation. Sequences for

509 all oligos to generate single guides, repair templates, and recombinant plasmids are
510 available upon request.
511
512 *Immunofluorescence*
513 Antibody staining of dissected gonads was as previously described[3]. DIC and
514 fluorescent images were acquired on a Zeiss motorized Axioplan 2 microscope
515 with either a 40x Plan-Neofluar (numerical aperture 1.3), a 63x Plan-
516 Apochromatic (numerical aperture 1.4), or 100x PlanApochromatic (N.A. 1.4)
517 objective lens using a AxioCam MRm camera and AxioVision software (Zeiss).
518
519 *Mosaic analysis*
520 To associate the somatic focus of action of *pod-2* for germline phenotypes, array
521 losses were characterized in animals of genotype *pod-2(1691null); tnEx212[W09B6-*
522 *pod-2(+)--20 ng/µl—hi copy; sur-5::gfp]* that were isolated on the basis of sterility.
523 Subsequently, potential candidate mosaics of interest were prescreened directly at
524 the dissecting microscope level for asymmetry in the phenotypic severity seen
525 between anterior and posterior gonad arms, and then examined at the compound
526 microscope level for loss of *sur-5::gfp* expression. Potential *pod-2(tn1691null);*
527 *tnEx219[W09B6-pod-2(+)–4 ng/µl—lo copy; sur-5::gfp]* genetic mosaics were also
528 prescreened in this manner. Intestinal (E–) mosaics were prescreened using low-
529 power fluorescence (Nikon SMZ18, with Lumencor SOLA Light Engine), but for *pod-2*
530 many of these candidate mosaics were seen to express *sur-5::gfp* at very low levels,

531 or in just a few intestinal cells, when examined at high power. This was not an issue

532 when isolating *fasn-1(tn1762null); tnEx218[fasn-1(+); sur-5::gfp]* E(–) mosaics.

Data availability

All *C. elegans* strains are available from the Caenorhabditis Genetics Center or by request. DNA sequences for all oligonucleotides used to generate single guides, repair templates, and plasmids are available upon request. All other data and materials supporting the findings of this study are available upon request.

Acknowledgements

We are grateful to our colleagues Gabriela Huelgas-Morales, Caroline Spike, and Tatsuya Tsukamoto for suggestions regarding experiments and comments on the manuscript. This work was supported by National Institutes of Health (NIH) grant GM57173 to D.G. Some strains were provided by the Caenorhabditis Genetics Center, which is funded by grant P40OD010440 from the NIH Office of Research Infrastructure Programs.

Author contributions

T.S. conducted the experiments, prepared the figures, and wrote the manuscript. T.S. and D.G. designed and conceptualized the research study. D.G. obtained funding, supervised the study, and edited the manuscript.

Competing interests

The authors declare no competing interests.

533 **Figure Legends**

534 **Figure 1**. Ovulation and oocyte development are delayed in *inx-8(rf).* **a**) Diagram
535 of adult *C. elegans* gonad. Posterior arm shows the positions of the somatic
536 distal tip cell (DTC) and five pairs of sheath cells (nuclei are numbered). Anterior
537 arm shows the underlying germline, approximate regions of germ cell
538 proliferation (Prolif.), meiotic pachytene stage (Pach.), and developing oocytes.
539 Embryos typically undergo some cell division in the uterus before being laid. Sp,
540 spermatheca; vul, vulva. **b**) Compared to wild type (N2), ovulation in *inx-8(tn1513*
541 *tn1555rf)* mutants (a.k.a. *inx-8[rf]*) is delayed ~18 hrs. Bars representing 1-3 hr
542 windows indicate approximate time of the fourth larval stage (L4 to adult) molt,
543 followed by time of appearance of the first fertilized embryo ovulated into the
544 uterus. **c)** Onset of *gfp::lin-41* expression as a marker of oocyte development is
545 delayed in *inx-8(rf)*. Panels show DIC images of vulval development (left), loop
546 region of gonad arm (middle), and expression of *gfp::lin-41* (right). Wild-type
547 hermaphrodites express *gfp::lin-41* by the approximate L4.7 sub-stage of vulval
548 development (vul); *inx-8(rf)* hermaphrodites do not express *gfp::lin-41* until after
549 vulval development is complete but before the L4-to-adult molt. Null *inx-*
550 *8(tn1474) inx-9(ok1502)* hermaphrodites, rescued for *inx-8::gfp* expression in the
551 DTC with *Ex[lag-2p::inx-8::gfp]*--a.k.a. *inx-8/9(0); Ex[inx-8(DTC+, Sh-)]* -- show a
552 similar delayed onset of *gfp::lin-41* expression as *inx-8(rf)*. Bar, 20 µm.

553

554 **Figure 2.** INX-8(T239I D24N) compromises gap junction formation between
555 soma and germline. **a**) Somatic INX-8 in wild-type (WT) gonads localizes to

556 puncta representing soma-germline gap junctions where DTC or sheath cells
557 overlie germ cells. **b)** In WT distal gonad arms, gap junction puncta aggregate in
558 small clusters associated with each germ cell; in *inx-8(rf)* distal arms, gap
559 junction puncta localize more apically, where sheath dips down between germ
560 cells, outlining the cell (honeycomb pattern). Localization of INX-21 and INX-22
561 define the two different classes of germline gap junction hemichannels, both of
562 which include INX-14 subunits. **c)** At the loop region, WT gap junction puncta
563 form large higher-order aggregates (arrows) which are absent in *inx-8(rf)*. **d)** In
564 WT proximal arms, gap junction formation with INX-22-containing hemichannels
565 is extensive; in *inx-8(rf)*, INX-22 and INX-8(T239I D24N) are strongly expressed
566 but show little evidence of gap junction formation. "–1" indicates the most
567 proximal oocyte; *inx-8(rf)* hermaphrodites frequently show undersized oocytes at
568 this position as well (<). **e**) Heterozygous *+/inx-8(rf)* shows little effect on gap
569 junction localization in an *emb-8(hc69ts)* background. Antibodies specific to INX-
570 8, INX-21, or INX-22 were used as indicated. DAPI-stained DNA in blue. Bar, 50
571 µm.
572
573 **Figure 3.** a**)** Predicted assignment of FAS mutants in a simplified FAS pathway.
574 Targeted deletions and GFP insertions are shown for *pod-2* (**b)** and *fasn-1* (**c**).
575 Predicted isoforms for POD-2 are indicated. **d-h**) Phenotypes of homozygous
576 mutant embryos from **d**) *+/pod-2(0)*; **e-h**) *fasn-1(0); Ex[fasn-1(+)]*. Arrow in (**d**)
577 indicates differentiated anterior pharynx; arrow in (**e**) indicates multiple ectopic
578 nuclei present at fertilization that persist during early stages of embryogenesis.

579 **Figure 4.** Wild-type INX-8 facilitates effects of *Ex[pod-2(+)]* overexpression on
580 conditional mutations downstream in the fatty acid synthesis (FAS) pathway.
581 Brood size was measured as the number of viable progeny produced. The
582 balancer *mIs11* provided *inx-8(+)* for all strains listed. **a**) Embryonic lethality in
583 *emb-8(ts)* mutants at 22°C is more severe in heterozygous *+/inx-8(rf)* than *inx-*
584 *8(+)* backgrounds *(1)*. Expression of *Ex[pod-2(+)]* in *emb-8(ts)* significantly
585 rescues embryonic lethality *(2)*. Rescue of *emb-8(ts)* by *Ex[pod-2(+)]* is also
586 dependent on *inx-8(+)* copy number *(3)*. **b**) Expression of *Ex[pod-2(+)]* in *fasn-*
587 *1(ts)* mutants at 20°C reduces brood size *(1)*. *fasn-1(ts); inx-8(+)* homozygotes
588 show greater embryonic lethality than *fasn-1(ts); (+)/inx-8(rf*) heterozygotes in the
589 absence *(2)* or presence *(3)* of *Ex[pod-2(+)]*. Averages indicated with dotted
590 lines. Probability was calculated using Student's 2-tailed *t*-test. **c**) Enzymes
591 (purple) implicated in germline FAS. Malonyl-CoA transits from soma sheath to
592 germline through gap junction channels comprised of INX-8/9 (soma) and INX-
593 14/INX-21 (germline) hemichannels. Germline FASN-1 uses malonyl-CoA to
594 synthesize palmitate, which may be further extended and modified to produce
595 other long-chain fatty acids. EMB-8 (NADPH-dependent CYP450 reductase) and
596 POD-7/8 (CYP450s) are necessary to synthesize the lipid-rich (inner) layer of the
597 eggshell and support polarity establishment[14,16]; the composition of lipid layer
598 fatty acids is unknown. *de novo* PUFA synthesis is required in the germline for
599 embryonic viability, and is implicated in sperm guidance[35,36]. The identities of
600 other long-chain fatty acids that may be synthesized in the germline are

601 unknown. PUFAs, polyunsaturated fatty acids; LFAs, long-chain fatty acids;
602 MUFA, monounsaturated fatty acids; pm, plasma membrane.
603
604 **Figure 5.** Genetic mosaic analyses of *pod-2* reveal a mal-CoA requirement in
605 somatic gonad sheath. **a**) Abbreviated cell lineage of *C. elegans*. Mosaics
606 characterized correspond to loss of *sur-5::gfp* expression in the germline (P_4),
607 intestine (E), or somatic gonad. Five *pod-2(0); Ex[pod-2(+); sur-5::gfp]* animals
608 lost the array from all somatic gonad sheath cells and produced no viable
609 embryos. **b**) Eight animals showed differences in array retention in each gonad
610 arm with phenotypic consequences. Arrays were generated by microinjecting
611 cosmid W09B6 *[pod-2(+)]* at 4 ng or 20 ng/µl (low/high copy). **c**) Uterus of non-
612 mosaic *pod-2(0); Ex[pod-2(+)*--high copy*]* hermaphrodite; developmental
613 progression of embryos from each gonad arm is comparable. **d**) Mosaic *pod-*
614 *2(0); Ex[pod-2(+)*--high copy*]* with array lost from posterior gonad arm sheath but
615 retained in a single Sh4 cell of anterior arm. Anterior arm embryos have more
616 distinct eggshells and develop to later stages. **e-h**) Embryonic development
617 depends on somatic levels of mal-CoA. Shown are terminal-stage *pod-2(0)*
618 embryos derived from parents of designated genotypes. **e**) Pretzel-stage embryo
619 from *+/pod-2(0)*. **f**) 3-fold stage embryo from *pod-2(0); Ex[pod-2(+)--low copy]*,
620 with array maintained in soma but lost in the germline (P4–). **g**) Pretzel-stage
621 embryo from P4(–) mosaic *pod-2(0); Ex[pod-2(+)--high copy]*. **h**) Embryo from
622 mosaic *pod-2(0); Ex[pod-2(+)--low copy]* with uncharacterized somatic loss of
623 array, but array retained in the germline (P4+). This parent produced exclusively

624 dead embryos. **i**) Typical terminal undifferentiated *fasn-1(0)* Pod embryo from
625 *fasn-1(0); Ex[fasn-1(+)]*. ant ute, anterior uterus; post ute, posterior uterus; v,
626 vulva; –1, most proximal oocyte. Bar, 20 μm.
627
628 **Figure 6**. Mosaic loss from the intestine of *pod-2*, but not *fasn-1,* leads to an
629 ARD-like gonad arm. **a**) E(–) genetic mosaic *pod-2(0); Ex[pod-2(+); sur-5::gfp]*
630 gonad arms (from same animal). Gonad arm on right partially outlined. **b**) Two
631 focal planes of a presumptive P_1(–) *pod-2(0); Ex[pod-2(+); sur-5::gfp]* mosaic with
632 constipated intestine. Upper plane (left) with partially outlined intestine; lower
633 plane (right) shows underlying distal gonad arm. int, intestine; p, pachytene
634 region; v, vulva. **c**) E(–) genetic mosaic *fasn-1(0); Ex[fasn-1(+); sur-5::gfp]* gonad
635 arm. –1, most proximal oocyte. Bars, 20 μm.

Table 1

Brood sizes suggest FA synthesis influences embryo output

Genotype	Larvae	Dead embryos	Total (embryo output)
Wild type (N2)	291±29 (n=33)	2±2	293±29
inx-8(rf)	108±40 (n=90)	11±6 (n=30)	119±42
inx-8/9(0); Ex[inx-8(DTC+,Sh-)]	2±2 (n=32)	19±13	20±14
pod-2(0); Ex[pod-2(+)] high copy (20 ng/µl)	164±50 (n=31)	118±41	282±59
pod-2(0); Ex[pod-2(+)] low copy (4 ng/µl)	91±24 (n=41)	156±37	247±50
fasn-1(0); Ex[fasn-1(+)	0.05 (n=80)	276±18 (n=16)	276±18
fasn-1(0);inx-8(rf); Ex[fasn-1(+)	17±15 (n=47)	43±27	60±37

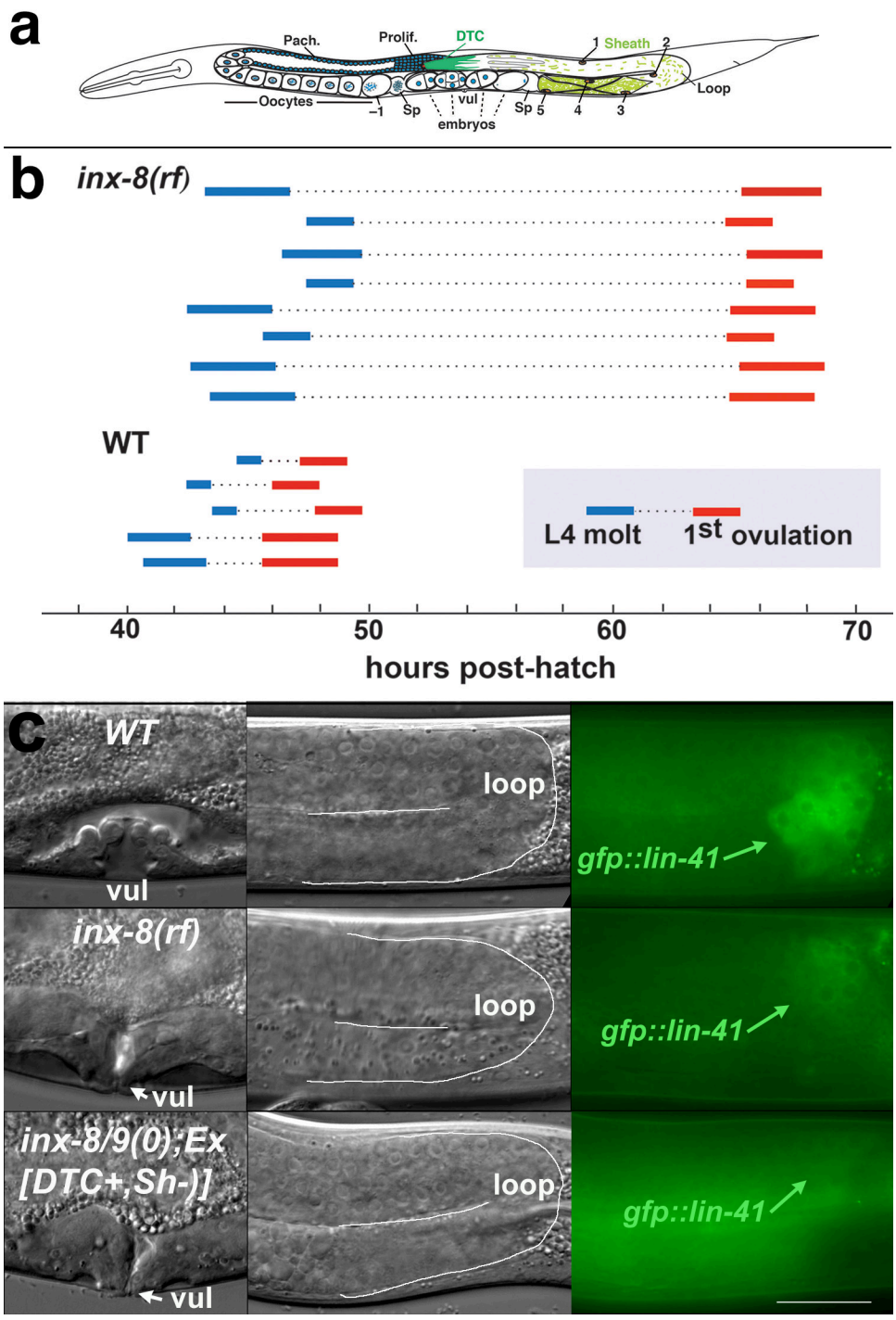
a
Pach.
Prolif.
DTC
1 Sheath 2
Loop
Oocytes
–1
Sp
vul
embryos
Sp 5
4
3
b
inx-8(rf)
WT
L4 molt
1st ovulation
40
50
60
70
hours post-hatch
c
WT
vul
loop
gfp::lin-41
inx-8(rf)
vul
loop
gfp::lin-41
inx-8/9(0);Ex
[DTC+,Sh-)]
vul
loop
gfp::lin-41

Figure 1

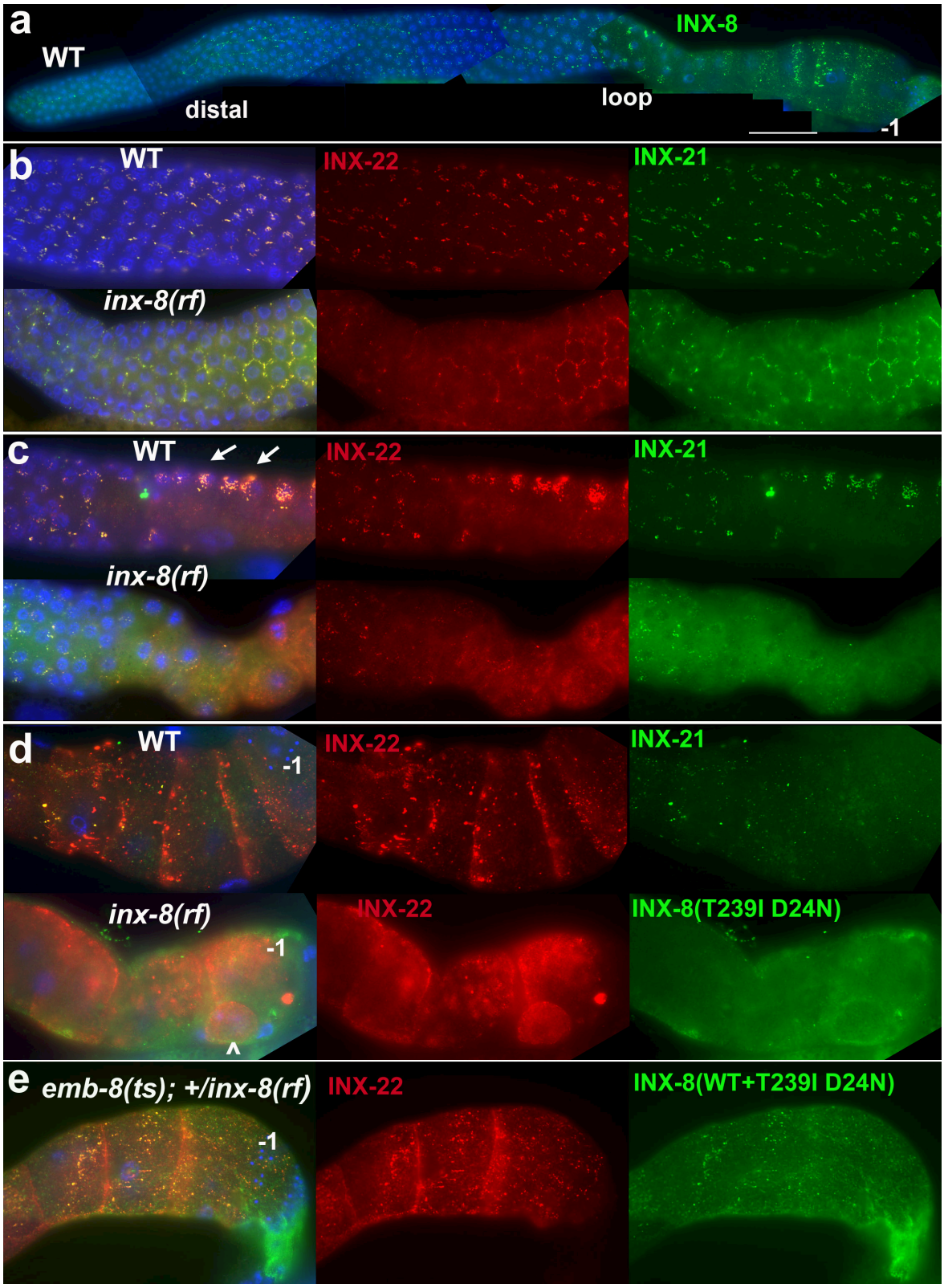
a
WT
INX-8
distal
loop
-1
b
WT
INX-22
INX-21
inx-8(rf)
c
WT
INX-22
INX-21
inx-8(rf)
d
WT
-1
INX-22
INX-21
inx-8(rf)
-1
INX-22
INX-8(T239I D24N)
e
emb-8(ts); +/inx-8(rf)
-1
INX-22
INX-8(WT+T239I D24N)

Figure 2

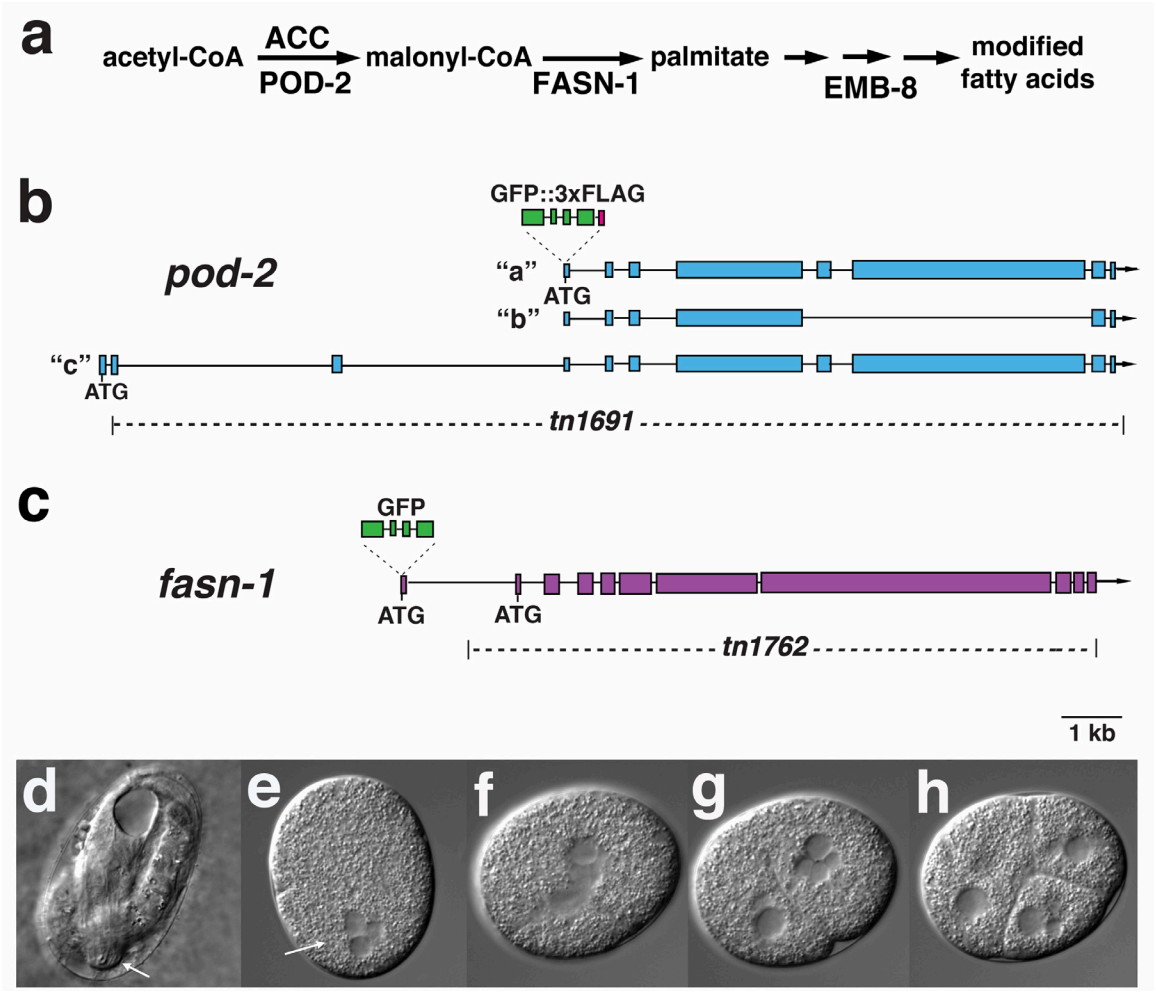
a
acetyl-CoA
ACC
POD-2
malonyl-CoA
FASN-1
palmitate
EMB-8
modified
fatty acids
b
GFP::3xFLAG
pod-2
"a"
ATG
"b"
"c"
ATG
tn1691
c
GFP
fasn-1
ATG
ATG
tn1762
1 kb
d
e
f
g
h

Figure 3

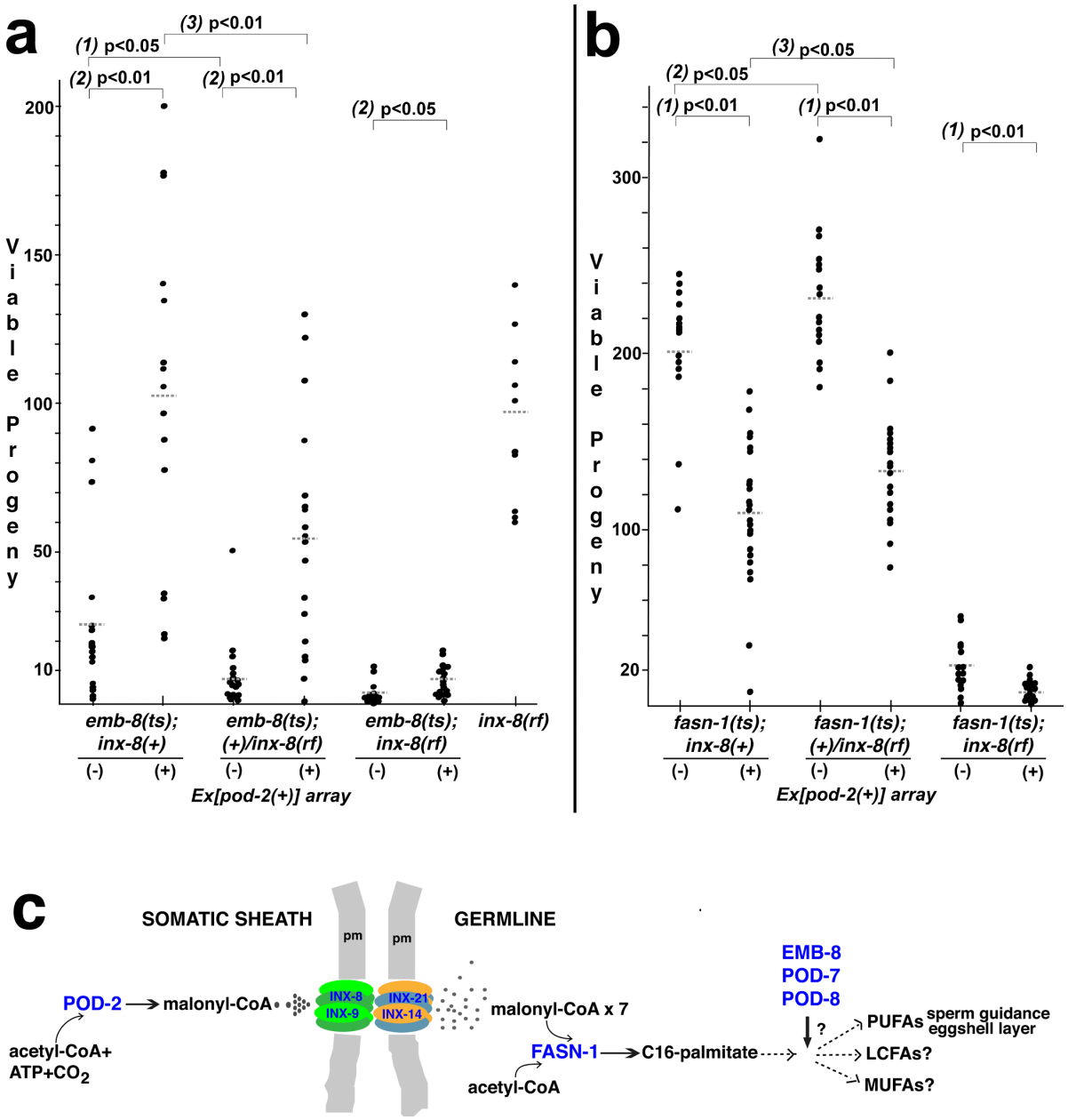
a
(3) p<0.01
(1) p<0.05
(2) p<0.01
(2) p<0.01
(2) p<0.05
Viable Progeny
200
150
100
50
10
emb-8(ts); inx-8(+)
emb-8(ts); (+)/inx-8(rf)
emb-8(ts); inx-8(rf)
inx-8(rf)
(-) (+) (-) (+) (-) (+)
Ex[pod-2(+)] array
b
(3) p<0.05
(2) p<0.05
(1) p<0.01
(1) p<0.01
(1) p<0.01
Viable Progeny
300
200
100
20
fasn-1(ts); inx-8(+)
fasn-1(ts); (+)/inx-8(rf)
fasn-1(ts); inx-8(rf)
(-) (+) (-) (+) (-) (+)
Ex[pod-2(+)] array
c
SOMATIC SHEATH
GERMLINE
pm
pm
INX-8
INX-9
INX-21
INX-14
POD-2
malonyl-CoA
acetyl-CoA+ ATP+CO2
malonyl-CoA x 7
FASN-1
C16-palmitate
acetyl-CoA
EMB-8
POD-7
POD-8
?
PUFAs
sperm guidance
eggshell layer
LCFAs?
MUFAs?

Figure 4

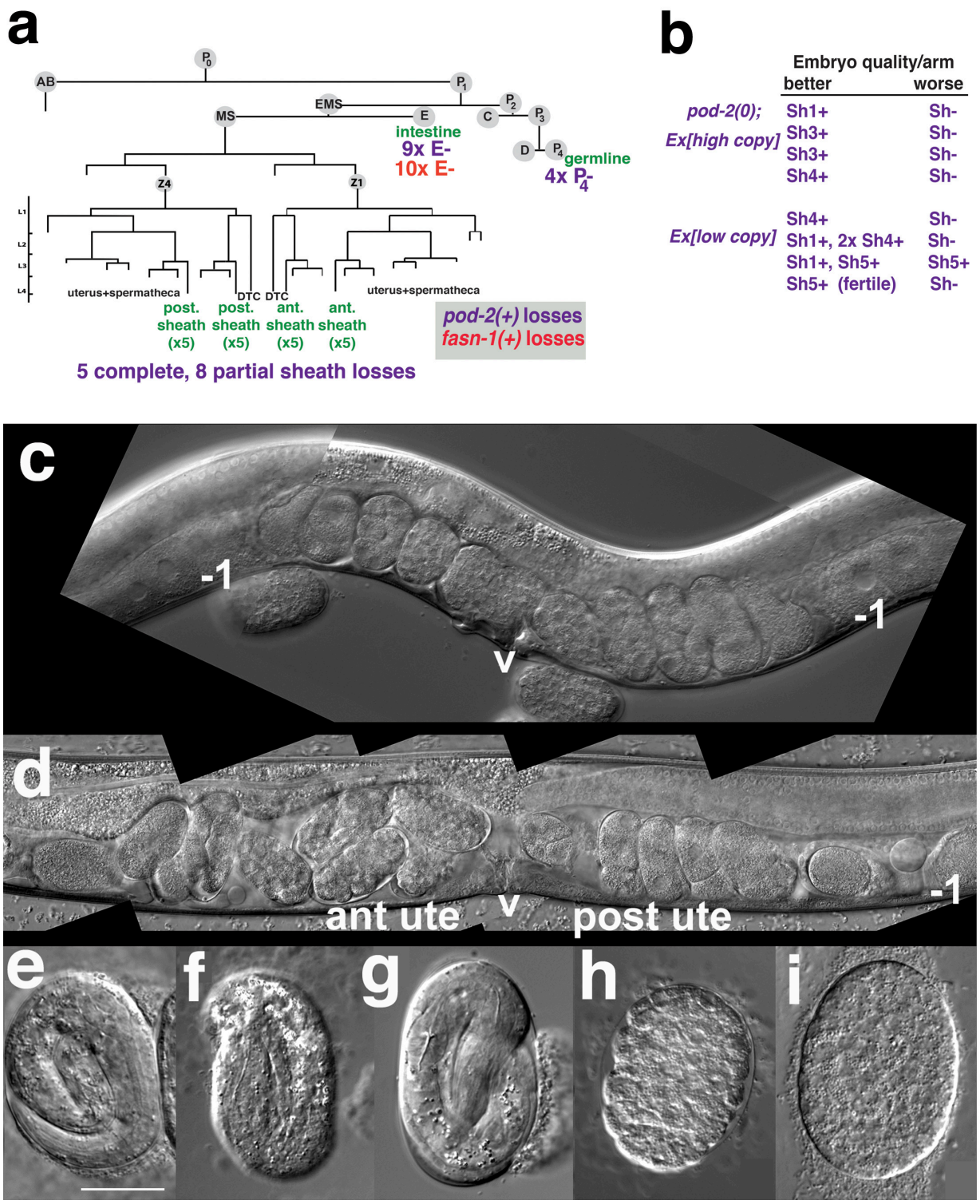
a
P0
AB
P1
EMS
P2
MS
E
C
P3
intestine
9x E-
10x E-
D
P4
germline
4x P4-
Z4
Z1
L1
L2
L3
L4
uterus+spermatheca
DTC DTC
uterus+spermatheca
post. sheath (x5)
post. sheath (x5)
ant. sheath (x5)
ant. sheath (x5)
pod-2(+) losses
fasn-1(+) losses
5 complete, 8 partial sheath losses
b
Embryo quality/arm
better
worse
pod-2(0);
Ex[high copy]
Sh1+
Sh3+
Sh3+
Sh4+
Sh-
Sh-
Sh-
Sh-
Ex[low copy]
Sh4+
Sh1+, 2x Sh4+
Sh1+, Sh5+
Sh5+ (fertile)
Sh-
Sh-
Sh5+
Sh-
c
-1
-1
v
d
ant ute
v
post ute
-1
e
f
g
h
i

Figure 5

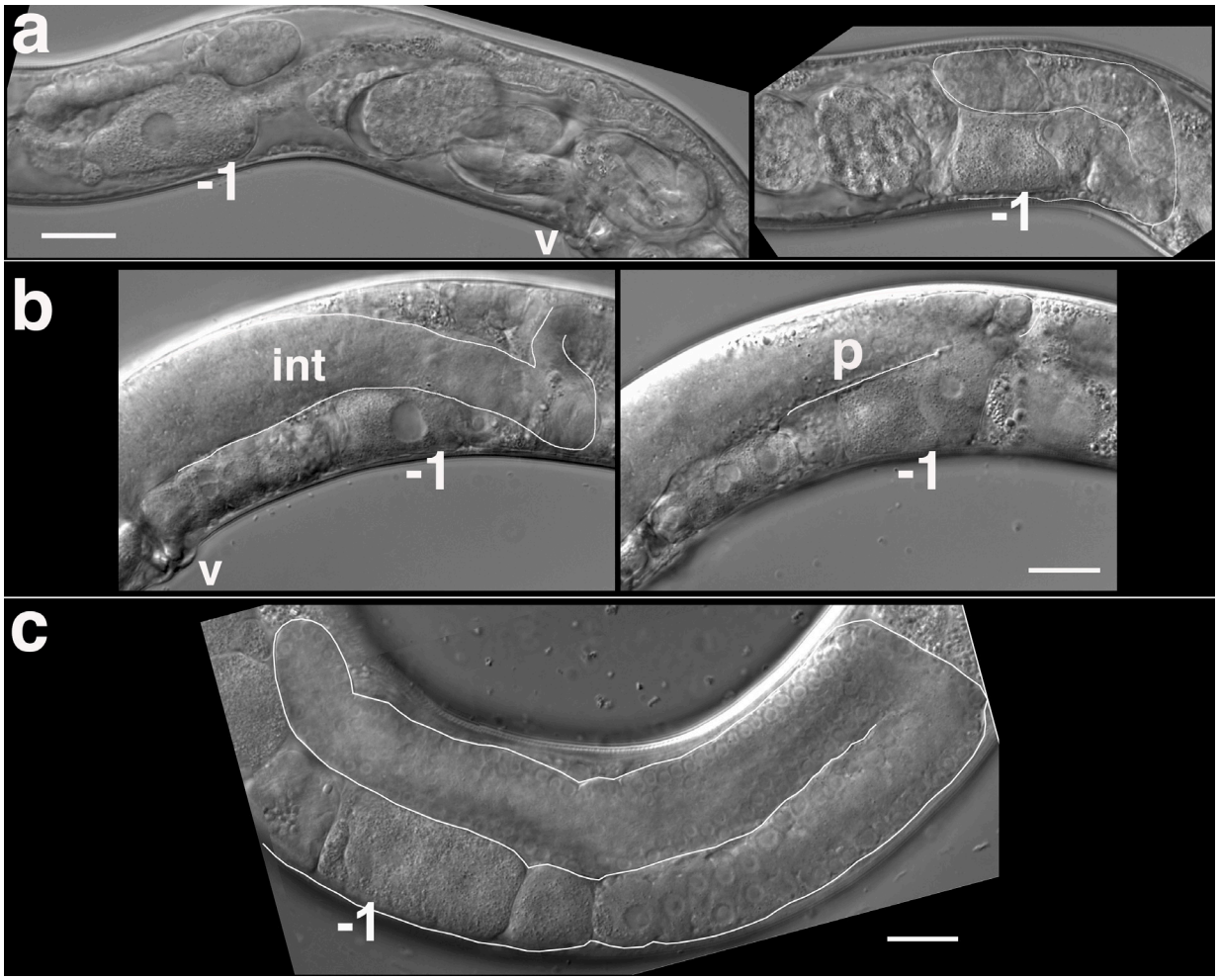

Figure 6

636

637 **Supplementary Information**
638
639 **Gap junctions deliver malonyl-CoA from soma to germline to support**
640 **embryogenesis in *Caenorhabditis elegans***
641

642 Todd A. Starich[1,2] and David Greenstein[1]
643 [1]Department of Genetics, Cell Biology and Development, University of
644 Minnesota, Minneapolis, Minnesota 55455 USA
645 [2]Email: stari001@umn.edu
646
647 Contents:
648 Supplementary Tables: 2
649 Supplementary Figures: 5
650 Supplementary Figure Legends
651 Supplemental References (46-49 in the list in the main text).
652

Supplementary Table 1

***inx-8(rf)* exhibits reduced brood size and interacts with FA synthesis pathway genes**

Genotype	Brood size	Germ cells per gonad arm
20°C		
N2 (wild type)	291±29 (n=33)	≥1000[46]
inx-8(rf)[1]	108±40 (n=90)	322±18 (n=3; day 2 adult)
22°C		
inx-8(+)[2]	266±40 (n=32)	
+/inx-8(rf)	255±36 (n=32)	
fasn-1(g43ts); inx-8(+)	115±41 (n=11)	
fasn-1(g43ts); +/ inx-8(rf)	114±47 (n=11)	
fasn-1(g43ts); inx-8(rf)	4.5±2.3 (n=12)	
emb-8(hc69ts); inx-8(+)	95±50 (n=15)	
emb-8(hc69ts); +/inx-8(rf)	35±37 (n=15)	
emb-8(hc69ts); inx-8(rf)	11±9 (n=15)	

[1]Full genotype *inx-8(tn1513 tn1555) inx-9(ok1502).* Approximately 4% of animals are infertile in one or both gonad arms (n=168).
[2]*inx-8(+)* provided on the balancer *mIs11* IV.

Supplementary Table 2

Reduced soma-germline gap junction coupling delays gametogenesis

a) *gfp::lin-41* expression at L4 vulval sub-stages

Genotype	L4.4	L4.5	L4.6	L4.7	L4.8	L4.9	L4.9< <molt
gfp::lin-41; inx-8(+)	1/11		3/3	5/6	5/6	4/4	
gfp::lin-41; inx-8(rf)		0/2	0/3	0/6		0/2	16/37
gfp::lin-41; inx-8/9(0); Ex[inx-8(DTC+,Sh-)]	0/11	0/3		0/2	0/1	0/3	6/14

b) sperm appearance at L4 sub-stages

Genotype	L4.4	L4.5	L4.6	L4.7	L4.8	L4.9	L4.9< < molt
N2	0/9	0/2	0/5	4/11	1/2	1/2	6/6
inx-8(rf)	0/3		0/1	0/2	0/3	0/1	1/10

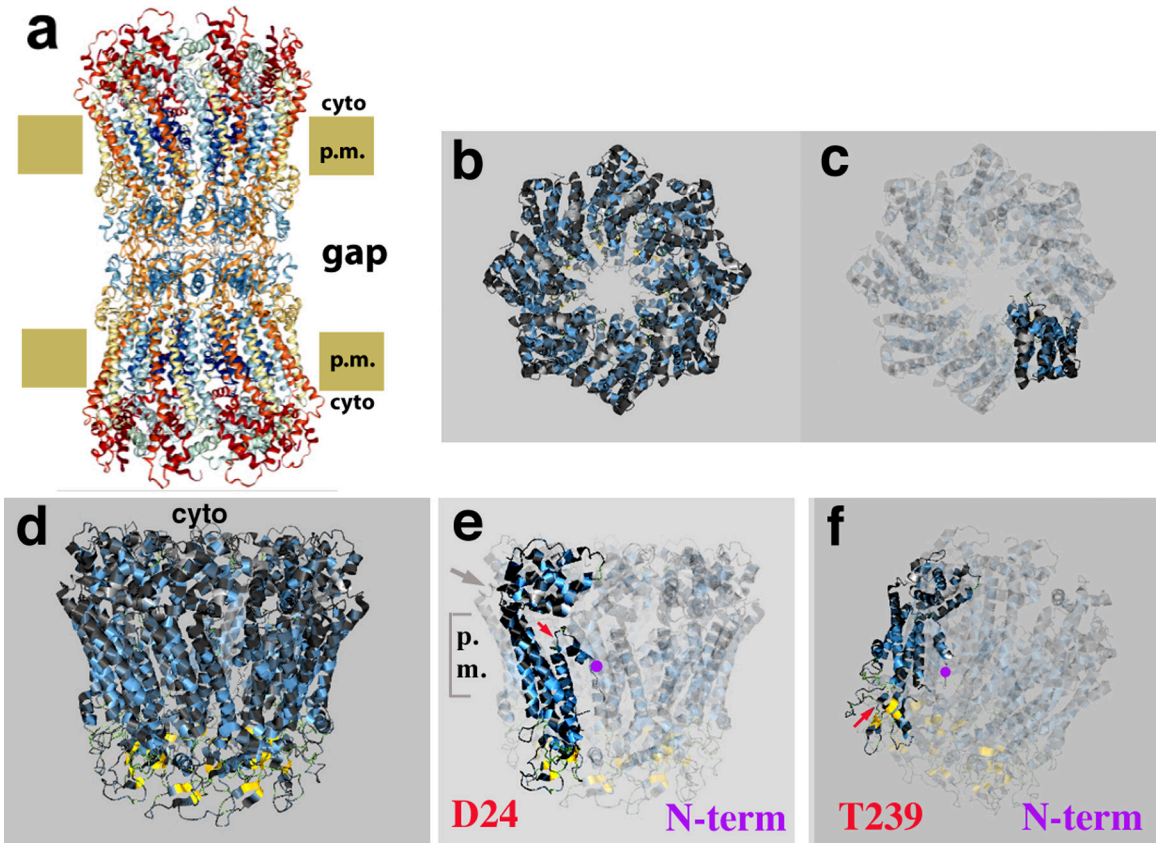

Supplementary Figure 1

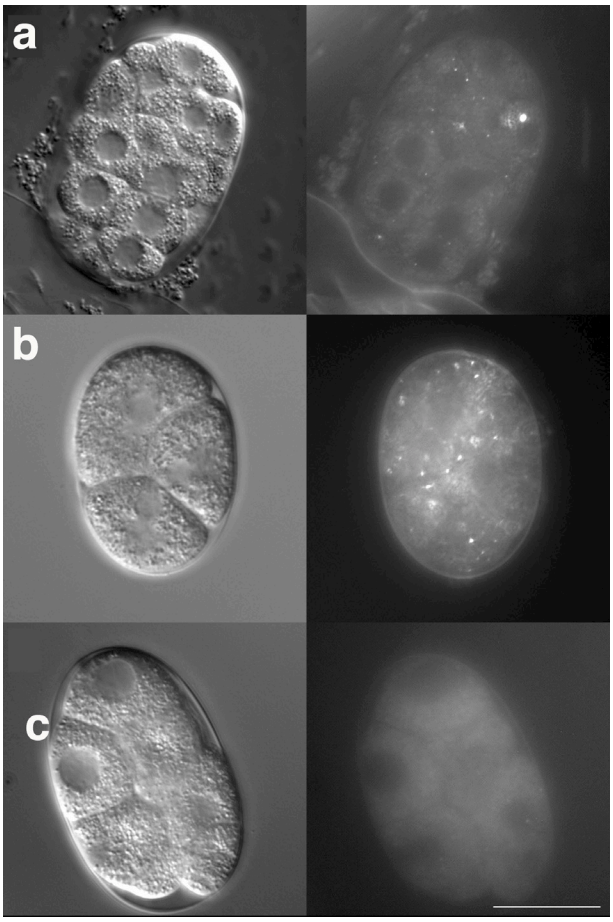

Supplementary Figure 2

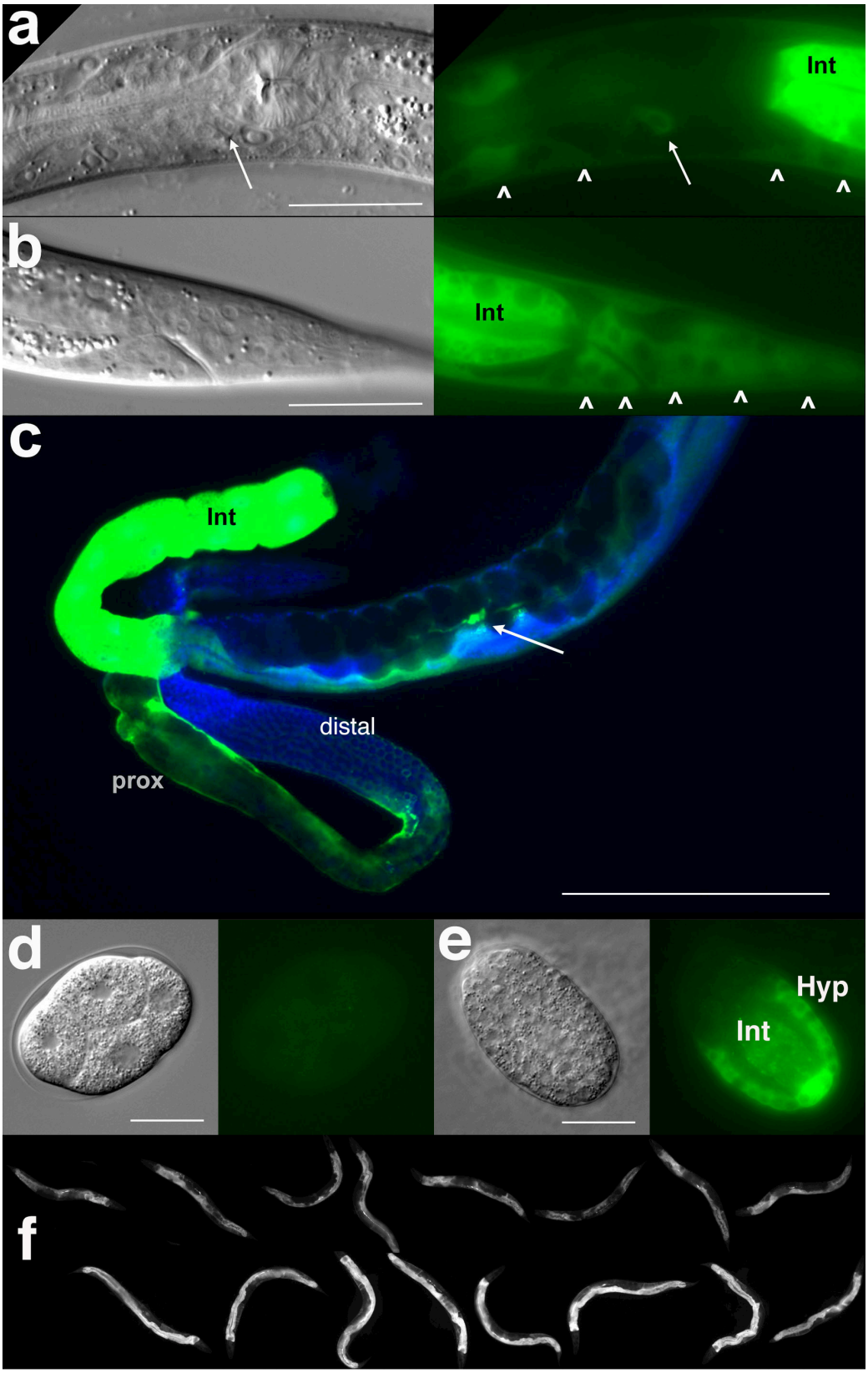

Supplementary Figure 3

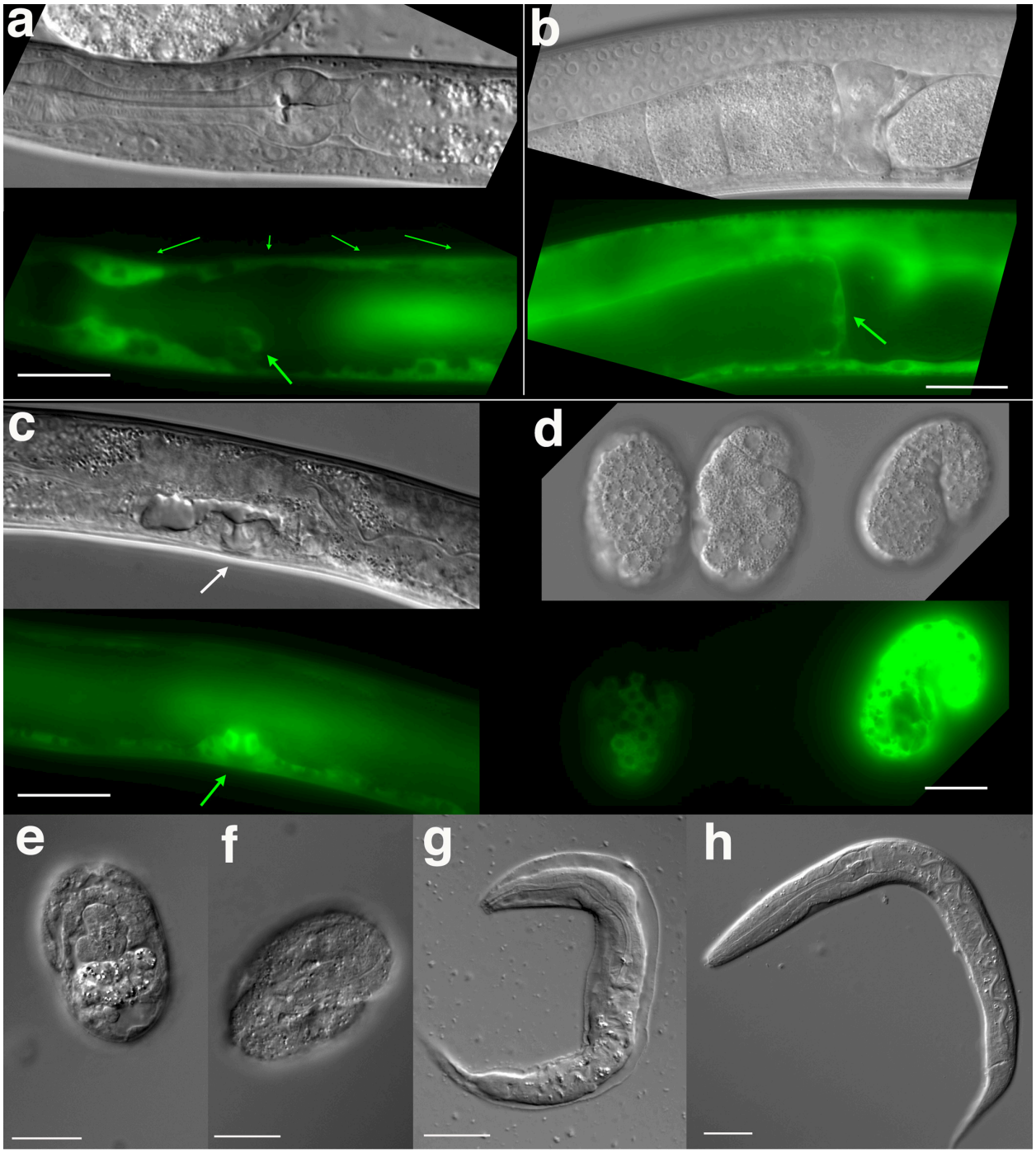

Supplementary Figure 4

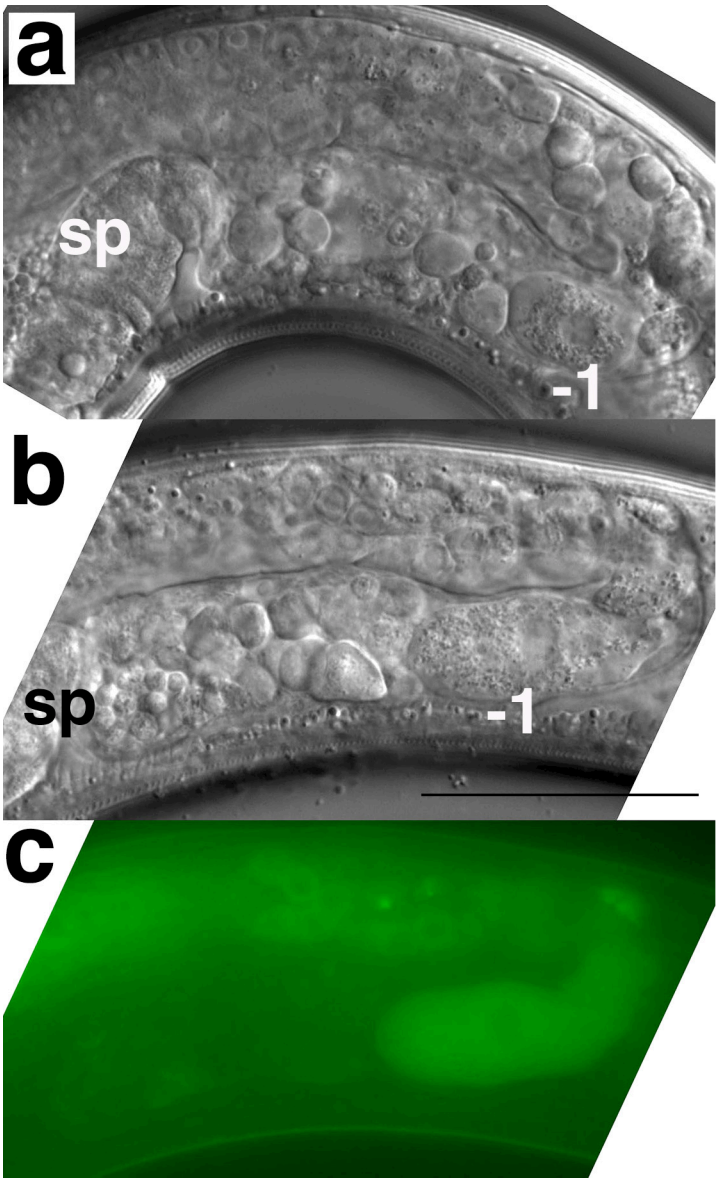

Supplementary Figure 5

653 **Supplementary Figure Legends**
654
655 **Supplementary Figure 1.** Predicted topological sites of amino acids mutated in
656 *inx-8(tn1513 tn1555) inx-9(0)*. **a**) Atomic structure of the *C. elegans* homomeric,
657 homotypic INX-6 gap junction full channel, determined by Oshima, *et al.*[19] (PDB
658 I.D. 5H1R, rcsb.org[47], viewed with NGL viewer[48]). Octameric hemichannels
659 associate via extracellular loops to form an enclosed channel in the region
660 classically identified by TEM as the "gap" between closely aligned plasma
661 membranes. cyto, cytoplasmic membrane face; p.m., plasma membrane. **b-f**)
662 Model for INX-8 hemichannel based on homology alignment to INX-6
663 (aquaria.ws). **b**) Cytoplasmic view. **c**) Single subunit highlighted. In wild type this
664 hemichannel is comprised of both INX-8 and INX-9 subunits, and associates with
665 germline hemichannels comprised of INX-14+INX-21 or INX-14+INX-22. **d**) Side
666 view of hemichannel. Beta-strands (yellow) in the extracellular loops contribute to
667 walling off the pore. **e**) Single subunit highlighted. Kinked region (gray arrow)
668 allows the cytoplasmic structure of the subunits (cytoplasmic loop and C-
669 terminus) to form a dome at the pore entry. Amino termini (N-term) line the pore
670 as a funnel; a loop in the amino terminus allows for an interaction with residues in
671 the dome[19]. D24 in INX-8 (red arrow) lies near the D21 residue predicted by
672 homology with INX-6 (D25) to interact with the cytoplasmic dome. **f**) INX-8 T239
673 is predicted to lie adjacent to a beta-strand contributing to hemichannel-
674 hemichannel association (red arrow). (To expose the extracellular loop region in
675 relation to "**e**", the aspect of view is rotated towards the viewer and angled up to
676 the left.)

677 **Supplementary Figure 2.** *inx-8(rf)::gfp* can be endocytosed by oocytes. **a**) *inx-*
678 *8(+)::gfp* expressed in the somatic gonad sheath is endocytosed during ovulation
679 and appears as distinct fluorescent puncta in early embryos. **b**) *inx-8(rf)::gfp*
680 expressed on an extrachromosomal array in *inx-8(0) inx-9(0)* animals is
681 endocytosed by ovulating oocytes. **c**) *inx-8::gfp* expressed by the DTC in *inx-*
682 *8/9(0); Ex[inx-8(DTC+,Sh-)]* is not observed in early embryos. Bar, 20 µm.
683
684 **Supplementary Figure 3**. GFP::POD-2 expression. **a)** Expression in the head
685 includes hypodermis (carets) and excretory duct cell (arrow). Int, intestine. **b**)
686 Primary expression in the tail includes hypodermis (carets) and intestine (Int).
687 Left panel DIC image, right panel GFP fluorescence in live animals. **c)** Dissected
688 animal stained with anti-GFP antibody shows abundant intestinal expression (Int)
689 and strong expression in proximal sheath of exposed gonad arm (prox) that
690 diminishes in the distal arm. No germline expression is seen in the distal arm
691 where germ cells are revealed due to the absence of sheath coverage. Arrow
692 indicates CAN neuron. DAPI-staining of DNA in blue. **d**, **e**) Earliest expression in
693 embryos is evident in developing hypodermis and intestine. **a, b, d, e**) DIC
694 images in left panels, live GFP fluorescence in right panels. Bars are 20 µm,
695 except (**c)** 200 µm. **f**) GFP::POD-2 is responsive to starvation. Top row, animals
696 briefly washed and transferred to bacteria-free NGM plates for 4 hours; lower
697 row, animals similarly-treated but fed.
698

699 **Supplementary Figure 4**. GFP::FASN-1 expression and *fasn-1(0)* embryonic
700 phenotypes. **a**) GFP::FASN-1 is expressed throughout the hypodermis (small
701 arrows). Excretory duct cell expression is also indicated (larger arrow). **b**) Arrow
702 indicates proximal gonad sheath expression. **c**) Arrow indicates developing
703 vulva. **d**) Earliest expression in developing embryos is seen in hypodermis. DIC
704 images in upper panels, live GFP fluorescence in lower panels. **e-h**) Terminal
705 phenotypes of *fasn-1(0*) embryos or larvae from *+/fasn-1(0)* parents. All bars, 20
706 µm.
707
708 **Supplementary Figure 5.** Expression of *gfp::pod-2* in the germline fails to
709 rescue *inx-8(rf)* phenotypes. **a**) Young (first-day) adult *inx-8(rf)* gonad arm. **b, c**)
710 Young adult *inx-8(rf)* gonad arm expressing *mex-5p::gfp::pod-2::tbb-2-3'UTR*.
711 The *pod-2* isoform in this construct corresponds to *gfp::pod-2* isoform "a" in Fig.
712 3. This isoform encompasses sequence homology to all of the enzymatic sites in
713 other ACC multi-functional enzymes. Sp, spermatheca; -1, most proximal oocyte;
714 bar, 50 µm.